Multi-body Dynamics Simulation and Analysis of Wave-adaptive Modular Vessels

John D. Fratello

Thesis submitted to the faculty of Virginia Polytechnic Institute and State University in partial fulfillment for the degree of

Master of Science
In
Mechanical Engineering

Mehdi Ahmadian, Chair
Leigh S. McCue-Weil
Saied Taheri

April 29, 2011
Blacksburg, Virginia

Keywords: Catamaran seakeeping, suspension dynamics, shock mitigation, multi-body dynamics simulation

Multi-body Dynamics Simulation and Analysis of Wave-adaptive Modular Vessels

John D. Fratello

Abstract

Catamarans provide vast deck space, high thrust efficiency, and excellent transverse stability, however, in rough conditions they can be susceptible to deck slamming from head seas or bow diving in following seas and a pitch-roll coupling effect that can lead to uncomfortable corkscrew motion under bow-quartering seas. A new class of catamaran called Wave-Adaptive Modular Vessels (WAM-V™) aims to help mitigate oceanic input from the cabin by allowing for the relative motion of components not common to classic catamaran design. This thesis presents a set of multi-body dynamics simulation models created for two active WAM-Vs™ along with analysis on their suspension characteristics. Both models provide conclusive and realistic results, with the final model being validated against on-water testing data from a 12-ft unmanned prototype WAM-V™.

The first of these simulations serves primarily as a tool to evaluate WAM-V™ response characteristics with respect to a variety of parametric variations. The modeling environment is highlighted along with details of the parametric simulation and how it was created. The results fall in line with our expectations and are presented along with analysis of the sensitivity of each parameter at three longitudinal locations. The final simulation attempts to model the response of a 12-ft unmanned surface vessel (USV) prototype of the WAM-V™ configuration. Testing data is collected, processed, and applied to the model for validation of its prediction accuracy. The results of the sea tests indicate that the simulation model performs well in predicting USV motions at sea. Future considerations for testing WAM-Vs™ can include changes in suspension and mass parameters as well as limiting particular degrees-of-freedom by making their joints rigid.

Contents

List of Tables v

List of Figures vi

Chapter 1 1

Introduction 1

1.1 A Broad Overview of Catamaran Characteristics 2

1.2 Wave-Adaptive Modular Vessel (WAM-V™) 4

1.3 Research Objectives 6

1.4 Approach 6

1.5 Outline 7

Chapter 2 8

Technical Background and Literature Review 8

2.1 Review of Common Displacement Hull Forms 8

2.2 Introduction to Wave Adaptive Modular Vessels 10

Chapter 3 12

Proteus Modeling 12

3.1 Proteus Details 12

3.2 Modeling Environment – SimMechanics 13

3.3 Proteus Modeling 16

3.4 Parametric Analysis 22

Chapter 4 32

Unmanned Surface Vessel Characteristics 32

4.1 USV Design Overview 32

4.2 Physical Property Measurement and Static Testing 35

4.3 USV Multi-Body Dynamic Model Development 35

4.4 Spring and Damper Modeling 37
Chapter 5 41
Unmanned Surface Vessel Dynamic Testing 41
5.1 Instrumentation 41
5.2 Test Setup 46
5.3 On-water Testing 48
5.4 Model Input Pre-processing 49
5.4.1 Noise Reduction 50
5.4.2 Acceleration Integration 54
5.5 Single Degree of Freedom Modeling and Results 59
5.6 Multi-Body Dynamic Simulation Results and Validation 62
Chapter 6 69
Concluding Remarks 69
6.1 Summary and Discussion 69
6.1.1 Parametric Analysis of Proteus 69
6.1.2 USV Modeling & Validation 71
6.2 Recommendations 72
Appendices 74
A. Acceleration Integration – Omega Arithmetic 74
B. USV Single-DOF Model 76
References 78

List of Tables

Table 3-1. Description of Modes of Input Motion to Proteus 24

Table 3-2. Percent Variation of Parameters 26

Table 3-3. Example of Sensitivity Results 26

Table 5-1. Wave Direction Relative to USV and Vessel Heading per Leg 47

Table 5-2. Summary of Events Completed During Testing 49

Table 5-3. Integration Filter Calibration Test Procedure 58

Table 5-4. Linear Damping Coefficients Tested for Assumption Validation 63

Table 6-1. Summary of Parametric Analysis Results 70

List of Figures

Figure 1.1. The sustention triangle shows that the primary lifting forces on vessels can be split into three primary categories: buoyancy, dynamic lift and powered lift [5]. 1

Figure 1.2. Fuel consumption predictions for comparable catamaran and monohull at full and light displacement [12]. 2

Figure 1.3. The Proteus is a WAM-V™ concept of catamaran which utilizes springs and a ball joint to help mitigate oceanic inputs to the cabin and improve passenger comfort. 4

Figure 1.4. The engine pods of Proteus are attached to the pontoons with a pivot joint that allows the pod to rotate about the lateral axis freely with respect to the pontoon. 5

Figure 2.1. Example of a SWATH hull form. The water line sits just above the lower hull at some point along the strut [11]. 9

Figure 2.2. The springs positioned above each pontoon/arch attachment provide for mitigation of the heaving and pitching motions inherent to catamarans. 10

Figure 3.1. A simple grounded mass-spring-damper system. 13

Figure 3.2. Representation of the MATLAB code used to solve the MSD system. 14

Figure 3.3. Representation of the Simulink code used to solve the MSD system. 15

Figure 3.4. The MSD system as depicted using SimMechanics. Notice the physical nature of the modeling environment. 16

Figure 3.5. A stock car rests atop the input pads at the shaker rig located at VIPER in Danville, VA. 17

Figure 3.6. The under-workings of a shaker rig involve very large numerically controlled hydraulic pistons used to excite the vehicle's suspension. 17

Figure 3.7. Leaf springs were replaced with cylinders to ease the process of dynamic force application within the SimMechanics environment. Top: front suspension / Bottom: rear suspension. 19

Figure 3.8. The SimMechanics model was organized to be visually comparable to the Proteus top-view appearance. 20

Figure 3.9. The suspension bases were only restricted from pitching rotations and were driven with vertical translations. Here the capital letters P and R stand prismatic and rotational axes, respectively. 21

Figure 3.10. The signal used to drive the parametric model removed as many discontinuities as possible. 24

Figure 3.11. Variance in output sensitivity percentage from front to rear of the chassis from heave input. 28

Figure 3.12. Variances in output sensitivity from front to rear of the chassis from pitch input.. 30

Figure 4.1. The USV retains representative architecture to Proteus with the obvious addition of rigid skis between the front suspension and rear arch attachment. 33

Figure 4.2. The rear joint of the USV utilizes a combined ball and shaft to allow it freedom to rotate about the transverse and vertical axes only. 34

Figure 4.3. A spherical joint was utilized to attach the front arch and suspension and to allow for properly constrained motion of the pontoons relative to one another. 34

Figure 4.4. The USV CAD model is much simpler in architecture than the Proteus model. 36

Figure 4.5. This graph depicts the averaged left and right side raw spring force data. 37

Figure 4.6. Non-linearities in the suspension stiffness arise from two major areas which are called out in this depiction of the left from suspension system on the USV. 38

Figure 4.7. This figure represents the final single spring force vs. displacement curve. The blue points represent measured data and the red points at either end represent estimated data. 39

Figure 4.8. The USV response to 2 inches of initial compression exhibits the low damping ratio. 40

Figure 5.1. The CompactRIO is completely reconfigurable, allowing for comprehensive customization. 42

Figure 5.2. The battery and CompactRIO were situated within a water resistant box. Twelve waterproof connectors and an Ethernet port were also installed. 42

Figure 5.3. Accelerometers were mounted close to each arch attachment atop the rigid skis..... 43

Figure 5.4. Linear potentiometers were used to measure spring deflection while testing. 44

Figure 5.5. A string pot was installed using a custom mount to retain linearity of the measurement for both directions of motion. 45

Figure 5.6. The tri-axial cabin accelerometer was mounted directly to the base plate within the water resistant box. 46

Figure 5.7. A star pattern was utilized to ensure that data was taken with waves striking the vessel at each of five important directions. 47

Figure 5.8. This visual example of the FFT averaging scheme utilizes three decimated time series' to collate into the final frequency spectrum. 51

Figure 5.9. A portion of pontoon accelerometer data showing the engine both off and on. 52

Figure 5.10. The dominant frequencies of the engine noise can clearly be identified. 52

Figure 5.11. The Butterworth lowpass filter clearly eliminates engine noise with little trouble. 54

Figure 5.12. Discretization of continuous time-series signals leads to errors when a trapezoidal integration scheme is applied. 55

Figure 5.13. Integration error can stem from things such as a DC offset or other dynamic variations in central tendency. 56

Figure 5.14. A damper dynamometer was outfitted with sensors to gather calibration data for the integration filter. 58

Figure 5.15. A 1-DOF model was developed to predict USV suspension response frequencies. 59

Figure 5.16. The spring force vs. displacement curve was simplified using 4 linear curve fits. The lower numbers in the figure represent statistical displacement percentiles from testing. 60

Figure 5.17. The frequency response of the linear spring potentiometer showcases both the input and suspension response frequencies. 61

Figure 5.18. Two seconds of linear spring potentiometer displacement data displaying both the impact and suspension response frequencies. 62

Figure 5.19. As the data from Figure 5.18 is manually analyzed, it reveals the same frequencies found from the Fourier analysis. 62

Figure 5.20. Variation of right front spring displacement response due to damping coefficient. 64

Figure 5.21. Variation of right front spring velocity response due to damping coefficient. 65

Figure 5.22. Variation in center of gravity vertical acceleration response due to damping coefficient. 66

Figure 5.23. In the time domain the USV simulation appears to very accurately represent the realistic testing measurements. 68

Figure B-1. The USV was modeled as a pinned-and-cantilevered beam with a spring opposite the pin……76

Chapter 1

Introduction

The purpose of this chapter is to familiarize the reader with various types of marine vessels with a special emphasis being put on the advantages and disadvantages of catamaran designs. The fundamental lifting forces acting upon a ship can be split into three categories as can be seen in the Sustention Triangle of Figure 1.1: displacement buoyancy, dynamic lift and powered lift. This scope of this discussion will be limited to vessels relying solely on water displacement buoyancy, which will be defined as craft whose lift comes as a result of static buoyancy and does not vary with increasing velocity.

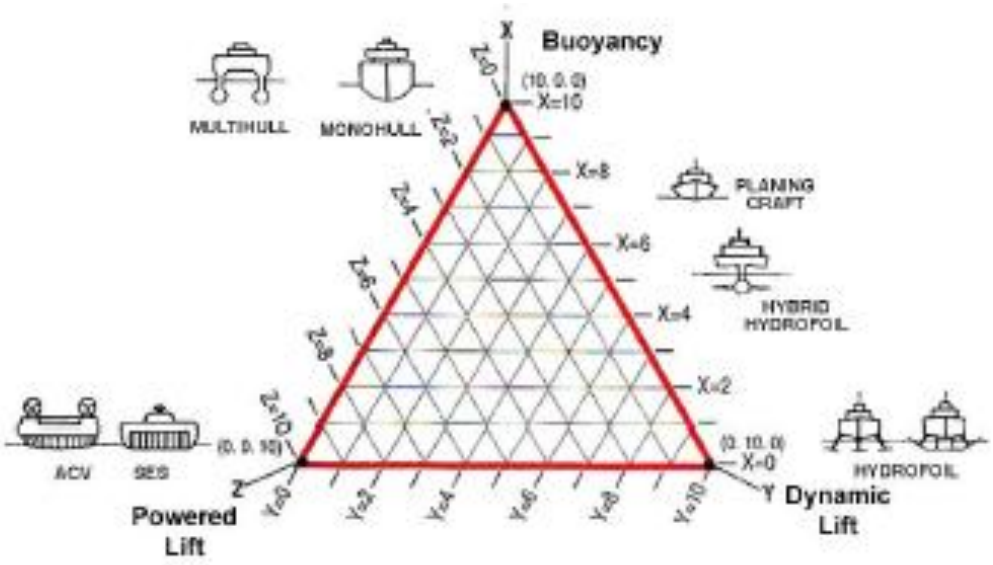

Figure 1.1. The sustention triangle shows that the primary lifting forces on vessels can be split into three primary categories: buoyancy, dynamic lift and powered lift. Used under Fair Use Guidelines, [5].

These displacement-type vessels can be split into two major categories: those with a single hull and those with multiple hulls. Catamarans are defined as two-hulled vessels whose primary flotation source rests at the water line. This concept can be extended to include various numbers of hulls including trimarans (three hulls) and pentamarans (five hulls), which begin to bridge the gap between single-hulled vessels and true catamarans in terms of lateral stability [4].

1.1 A Broad Overview of Catamaran Characteristics

Catamarans have several inherent advantages over standard monohull designs; however their application in seaways can be limited. Due to their geometry, catamarans can have much larger deck area and enjoy greater roll stability than a comparative displacement monohull vessel [5, 7, 8, 11, 14]. A properly designed catamaran can produce similar roll accelerations to a monohull [7] with rolling amplitudes 2.5 times smaller [10]. Catamarans have larger wetted area than comparable monohulls, which will lead to increased parasitic drag, but they generally require less total propulsive power due to their high aspect ratio hulls that can reduce wave resistance and therefore fuel consumption [5, 7, 13]. This effect is especially pronounced at higher speeds where wave resistance makes a greater impact as can be seen in Figure 1.2 below [12]. If equipped with individually-operated propulsors for each pontoon the catamaran can benefit from increased maneuverability via differential thrust [12] and a fault tolerance should an engine fail while underway.

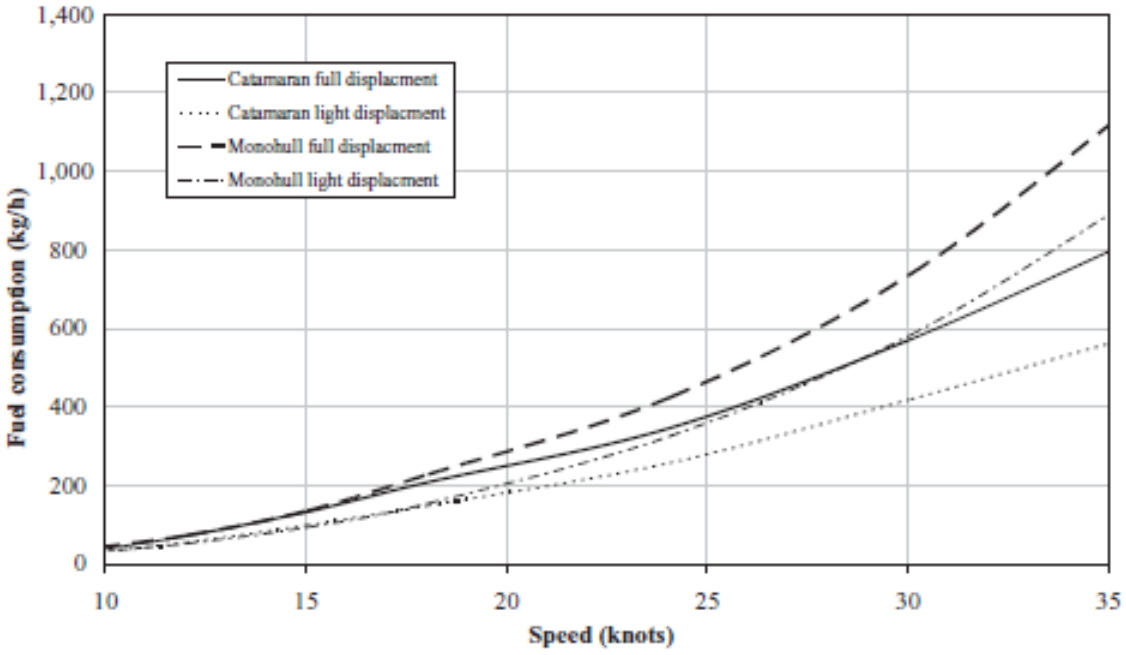

Figure 1.2. Fuel consumption predictions for comparable catamaran and monohull at full and light displacement. Used under Fair Use Guidelines, [12].

Catamarans do, however, come with a slight set of drawbacks as well. Baitis, et al. [1] concluded that a catamaran produced the worst seakeeping results as compared to three

monohulls and two SWATHs all designed for the same mission. Another consideration of great importance is their susceptibility to wet deck slamming in rough seas which can cause passenger discomfort or structural damage to the vessel [3, 5, 8, 9, 10, 11, 14]. Varyani, et al. [14] created a three-dimensional computational model to analyze the loads for a slamming incident in a catamaran drop test. They concluded that the narrow hull forms resulted in small magnitude loads while those encountered by the cross structure from its impact with the water can be quite large. Bonafoux, et al. [3] found that slam occurrences begin as significant wave height approaches the wet deck clearance, but a decrease from full speed actually increases the occurrence of slamming events. Fang and Chan [9] stated that catamarans can also be prone to bow diving in strong following seas.

Several studies have been performed to analyze the motion sickness incidence (MSI) or various vessels. Bonafoux, et al. [3] compared the motions of a monohull, catamaran, and pentamarans all of identical payload capacity. Their results indicate that the catamaran has the worst MSI in head and bow quartering seas, but performs the best of the three in beam seas. Davis and Holloway [6] modeled the response of several catamarans, trimarans, SWATHs, and monohulls using time domain strip theory. They concluded that in high seas the catamarans and SWATHs performed about the same with an approximate MSI of 50% to 70% while the monohulls and trimarans showed much better results with an MSI range of 40% to 50%. At lower significant wave height the SWATHs produced the least MSI at 0% to 5%, the monohulls and trimarans 5% to 10%, and the catamarans 5% to 15%. Turan, et al. [13] did work to produce a better model to estimate MSI from data recorded on vessels, which found that lateral acceleration plays an important role in the generation of sea sickness. During their tests they also discovered that lateral and vertical RMS accelerations at various locations on the vessel are equivalent for the catamaran, while the lateral acceleration of a monohull is approximately half that of the vertical acceleration.

Due to the high transverse stability of catamarans they can have similar natural roll and pitch frequencies. When encountering bow quartering seas, an out-of-phase dynamic coupling can occur in pitch and roll creating a corkscrew motion [5, 10, 12]. Another downside to this high stability is that at large roll angles the righting moment becomes very strong, which can create elevated roll accelerations [10].

1.2 Wave-Adaptive Modular Vessel (WAM-V™)

Several designs have been developed to help mitigate oceanic input into catamarans. Some of the more common methods involve the use of subsurface hydrofoils or stabilizing fins to add vertical damping to the system and alleviate some of the buoyant forces at work in high seas. Another concept which has been developed is the wave-adaptive modular vessel (WAM-V™), which retains the inherent advantages in speed and range afforded to a catamaran while supplying methods to help alleviate oceanic inputs and improve passenger comfort. This novel concept combines two innovative ideas on catamaran design. The first is the use of springs to attach the pontoons to the superstructure. This provides a flexible structure which can store and dissipate energy during the motion caused by waves. The second design innovation is the installation of a spherical joint between the main cabin structure and the front arch. This allows the front arch to rotate freely with respect to the cabin in turn providing independent motion of the front of either pontoon with respect to the other. Figure 1.3 depicts a 100-ft prototype WAM-V™ named Proteus.

Figure 1.3. The Proteus is a WAM-V™ concept of catamaran which utilizes springs and a ball joint to help mitigate oceanic inputs to the cabin and improve passenger comfort. Photo by author, 2011.

These advancements may help in terms of passenger comfort, but the architecture of WAM-Vs™ still leaves them susceptible to several potential problems. Proteus is propelled from engine pods mounted to the aft of each pontoon. Pivot joints attach the pods to the pontoons and allow for the engine pod to pitch freely with respect to the pontoons as can be seen in Figure 1.4. The goal of this design is to allow the propellers to stay in contact with the water as the aft of the vessel crests waves. As the engine pod pitches, however, the thrust vector changes direction, which produces oscillating surge accelerations felt at the cabin. This propulsion layout could also make it difficult to utilize water jets, which are much more efficient at high speed. The linear velocity at the tips of propellers can cause cavitation at speeds exceeding 30 knots whereas the impellers of a water jet propulsion system remain effective [10].

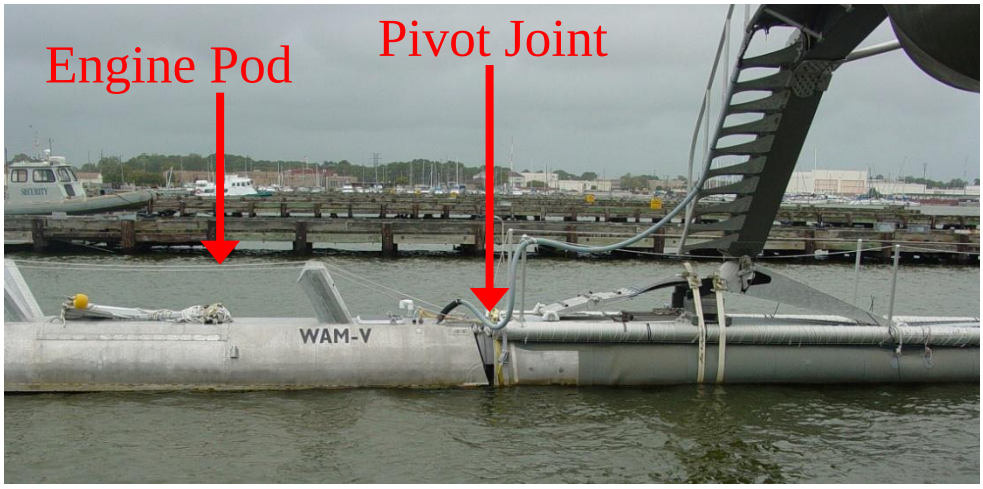

Figure 1.4. The engine pods of Proteus are attached to the pontoons with a pivot joint that allows the pod to rotate about the lateral axis freely with respect to the pontoon. Photo by author, 2011.

Another potential downfall of the WAM-V™ concept stems from the utilization of the suspension itself. As the springs compress, the cross structure clearance to the water line reduces, which could induce an increased number of slamming events to the lower cabin structure in high seas. However, these impacts will likely not be of the order felt in a standard catamaran with an enclosed center tunnel because the water will have an escape route once it strikes the cabin and the pressure spike should dissipate quickly.

1.3 Research Objectives

The primary objectives of this study are:

1) create a dynamic simulation model and perform analysis on the 100-ft prototype Proteus' suspension characteristics,
2) perform similar modeling on 12-ft unmanned prototype WAM-V™, instrument and perform testing on actual vessel, and validate test data to simulation,
3) characterize basic response parameters of the 12-ft unmanned surface vessel (USV) using simple models and validate with testing data, and
4) provide recommendations for future studies on WAM-Vs™.

1.4 Approach

During the course of this research, two main dynamic simulation models were created. Both models captured the vertical dynamic motion of the cabin with respect to pontoon action. The first model was kinematically accurate to the Proteus and was used to characterize parametric sensitivities on that particular vessel. The second was a simpler model used to mimic the prevalent characteristics of the 12-ft USV and was employed as a validation tool for the usage of dynamic simulations on these hull forms in replacement of testing. To defend these validating arguments the USV was carefully instrumented and tested on open water. A simple model was used to compare natural frequency estimation of the USV suspension with frequency response data recorded while testing. Based upon the results presented from these analyses, further modeling and prediction recommendations are made for these vessels.

1.5 Outline

Chapter 2 briefly outlines the technical background of various displacement hull forms and their seakeeping characteristics, as well as a primer on essential WAM-V™ architecture. Chapter 3 covers the principle characteristics of Proteus as well as the dynamic simulation development and results from a parametric analysis of its suspension. Chapter 4 details the primary variations of the USV from Proteus as well as the dynamic model created to represent it and the physical measurements made to ensure its accuracy. The USV instrumentation, testing, data pre-processing and validation discussion are presented in Chapter 5. Chapter 6 summarizes the work that was completed and provides recommendations for future prediction algorithms of WAM-V™ dynamics.

Chapter 2

Technical Background and Literature Review

The purpose of this chapter is to introduce the reader to the advantages and disadvantages of several types of marine displacement hull forms. A discussion is presented comparing the benefits and downfalls of monohulls, catamarans, trimarans, pentamarans and SWATH vessels. Specific emphasis is placed on the trade-offs between deck space, stability, speed, fuel efficiency (range) and seakeeping. Lastly, the primary goals of wave adaptive modular vessels are presented along with the variations from classic catamaran design required to create them.

2.1 Review of Common Displacement Hull Forms

The majority of marine vessels in use today rely primarily upon the lift created by the displacement of water to stay afloat. As discussed previously, multihulled ships have several distinct advantages over monohulls including greater deck area, excellent transverse stability, and less required power for a given speed. By varying hull shape and number, multihulls can take various forms that produce vastly different characteristics. Catamarans are twin-hulled vessels whose primary buoyant structure rests at the water line. A broad discussion of the advantages, disadvantages, and characteristics of catamarans was presented in section 1.1. The small-waterplane-area twin-hull (SWATH) utilizes two fully submerged submarine-like hulls attached to the superstructure with high aspect ratio streamlined struts as can be seen in Figure 2.1 [11]. This reduces submerging stiffness because the struts at the water line have very low volumetric displacement per vertical motion, thereby reducing oceanic inputs to the cabin. Trimarans and pentamarans are three- and five-hulled vessels, respectively, and they are thought to have an intermediate transverse stability between monohulls and catamarans [4].

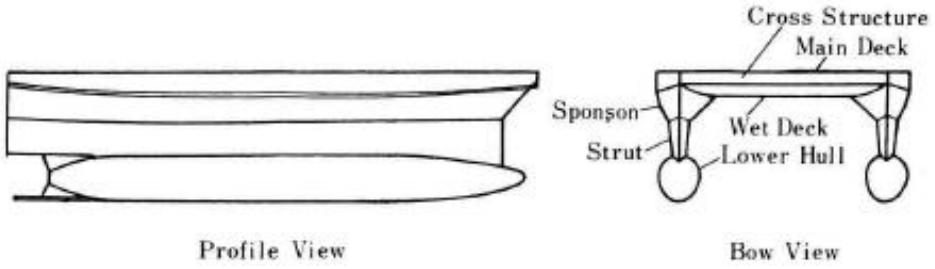

Figure 2.1. Example of a SWATH hull form. The water line sits just above the lower hull at some point along the strut. Used under Fair Use Guidelines, [11].

The high stability offered to catamarans can sometimes become problematic at high sea states because the righting forces on the vessel are very strong. SWATHs retain many of the advantages of catamarans while bettering passenger comfort, however, this only plays a significant role at higher sea states [6]. SWATHs suffer from much higher levels of resistance than a standard catamaran due to increased underwater surface area. This also results in top speeds much slower than a comparable catamaran [10]. By the nature of their architecture and construction, SWATH vessels will run a deeper draft and cost more to manufacture than a classic catamaran [10].

Trimarans and pentamarans have greater transverse stability than comparable monohulls. To attain this, lateral outriggers are mounted aside a primary central hull form. The increased resistance can be tuned to reduce wave resistance with proper lateral and longitudinal outrigger offset or frictional resistance by utilizing shallow outrigger hulls to decrease wetted area. When shallow outriggers are used, nonlinearity can arise in the roll stabilizing moment response because the unladen outriggers emerge from the surface at very moderate roll angles. This discontinuity produces two attractors at a single forcing frequency. When excited with this natural roll period, attractor jumping can be witnessed between large amplitude resonance and low amplitude anti-resonance depending on the initial conditions [4]. Another downside to running shallow draft outriggers on these vessels is that propulsion most likely will come from a single source on the central hull, which limits their maneuverability with respect to the differential power steering capabilities of catamarans. Both of these issues can be mitigated by using much deeper outrigger hull forms, but that comes at the expense of increased resistance. Bonafoux, et al. [3] studied the seakeeping characteristics of a monohull, catamaran, and pentamaran in various wave incident directions. They found that the pentamaran had the least

motion sickness incidence in head seas, equivalent to the monohull and better than the catamaran in bow quartering seas, and the worst MSI of the three in beam seas.

2.2 Introduction to Wave Adaptive Modular Vessels

The concept of a wave adaptive modular vessel (WAM-V™) came about in an effort to reap the many advantages inherent to catamarans while mitigating many of the unwanted responses characteristics also common to those designs. The most visually prevalent design concept of these vessels is the suspension system installed between each arch/pontoon attachment. Figure 2.2 depicts the right front suspension of the 100-ft WAM-V™ Proteus, which was illustrated in Figure 1.3. The suspensions act to store and dissipate the pitch and heave energy produced at the pontoons, thus reducing those motions as they are felt at the cabin.

Figure 2.2. The springs positioned above each pontoon/arch attachment provide for mitigation of the heaving and pitching motions inherent to catamarans. Photo by author, 2011.

In an effort to reduce the common coupling between pitch and roll exhibited in catamaran seakeeping and to allow the vessel to easily absorb quartering waves (those which produce pitching and rolling motions simultaneously) an innovative approach was taken to WAM-V™ superstructure design. Rather than forcing the pontoons to remain parallel with rigid attachments front-to-back and side-to-side, a spherical joint was installed between the main cabin and front

arch. This allows the front arch to rotate freely (primarily about a longitudinal axis passing through the joint) with respect to the cabin and rear arch, thus enabling the front of each pontoon to move separately from the other. In the automotive industry this would be commonly referred to as a system with zero warp stiffness, or negligible resistance to twisting between the front and rear of the vessel.

Due to the relative youth of the WAM-V™ concept, only one known document exists with relevant information, which is a NAVSEA Technical Memorandum on the propulsion and seakeeping characteristics of Proteus [2]. Calm water propulsion tests indicated that Proteus has a range of 1340 nautical miles at a full speed of 23 knots in both the light- and heavy-load cases. The seakeeping trials produced very interesting results. A beating phenomenon was present in nearly all of the time series signals, which was attributed to longitudinal propulsion variations from engine pod thrust vector angular displacement as well as propeller emergence as the pods crested over steep waves. This result is consistent with the subjective observation of strong longitudinal acceleration variations felt at the cabin. Throughout the trials the front suspension showed a strong tendency to bottom out onto the pontoon when the approaching swell period created sequential impacts in-phase with the cyclic pitch motions of the craft. The reason such extreme suspension motions occur comes down to the softening resistance nature of this leaf spring configuration. As the spring is depressed, the rate of vertical force generation actually decreases. The bottoming events create large vertical acceleration spikes at the cabin, with the greatest magnitudes being observed when both front suspensions bottom out simultaneously. In fact, vertical accelerations at the coxswain's seat generally stay below 0.5 g unless a simultaneous bottoming event occurs, in which case the maximum recorded acceleration reached 1.28 g. Their analysis shows that a spring redesign could maintain seat accelerations below 0.45 g in 4.3 ft seas at 10.3 knots. This study was sponsored by ONR 331 program manager, Ms. Kelly Cooper. Inquiries about this technical memorandum should be directed to NAVSEA Naval Surface Warfare Center, Carderock Division, Detachment Norfolk, 2600 Tarawa Court, Suite 303, Virginia Beach, VA 23459-3239. To the author's best knowledge the only WAM-Vs™ in existence are Proteus, three iterations of a 12-ft unmanned vessel, and a 33-ft version currently in development. Inquiries about WAM-V™ can be directed to Dr. Isabella Conti, Marine Advanced Research, Inc., 30 Railroad Ave., Unit 1, Point Richmond, CA 95801.

Chapter 3

Proteus Modeling

As discussed in Chapter 2, WAM-Vs™ could potentially produce incredible efficiency with a versatile arrangement while still providing sound seakeeping. However, unlike the vast majority of suspended vehicles, namely automobiles, the trends associated with tuning WAM-V™ parameters is entirely undocumented. This chapter is concerned with the development of a dynamic simulation model and the analyses used to help understand these parametric trends. The discussion will begin with brief details about the 100-ft prototype WAM-V™ named Proteus, which was designed by Marine Advanced Research (MAR) and will be the topic of this modeling effort. The SimMechanics environment is presented with comparison to other methods of solving dynamic systems along with elaboration on the application of Proteus into this environment. Finally, a parametric analysis is laid out for the Proteus model and concluding remarks are made on its derived trends.

3.1 Proteus Details

Proteus is a large lightweight catamaran which utilizes a novel design involving ball joints and springs in an effort to mitigate the transfer of sea motions from the pontoons to the cabin. This design has an approximate overall length of 100 ft and beam of 50 ft and utilizes two Cummins MerCruiser QSB5.9 marine diesel engines powering Arneson ASD-8 surface drives from external engine pods attached to the rear of each pontoon. Large titanium leaf springs are attached to rocker arms at the front and rear of each pontoon to create the suspensions. Above each suspension is connected a large aluminum arch used for supporting the cabin. The rear arch is rigidly connected to the superstructure (payload and cabin) while the front arch attaches with a large spherical joint. The primary purpose of this joint is to allow rotation of the front arch with respect to the superstructure about a longitudinal axis passing though the joint's center, although minimal rotation about the other axes must occur due to kinematic constraints. This joint

effectively allows the front of each pontoon to translate relative to one another freely and without necessarily resulting in motion at the cabin.

3.2 Modeling Environment – SimMechanics

Dynamic modeling of the Proteus was conducted in a programming environment known as SimMechanics, which is part of an addition to the Mathworks' MATLAB and Simulink suite of tools and is an object-oriented multi-body dynamics simulator. In order to better understand the visual nature of this program and its intuitive layout, a simple system will be discussed and analyzed using several methods.

Consider for a moment the simple mass-spring-damper (MSD) system depicted in Figure 3.1. This basic dynamic system can be easily solved analytically, numerically or by dynamic simulation. For the analytical and numerical solutions, the first step is to define the differential equations of motion (EOM). By solving the force balance on the mass with a free body diagram, the EOM can be solved as seen in equation (3-1).

$$\ddot{x} + \frac{c}{m}\dot{x} + \frac{k}{m}x = 0 \tag{3-1}$$

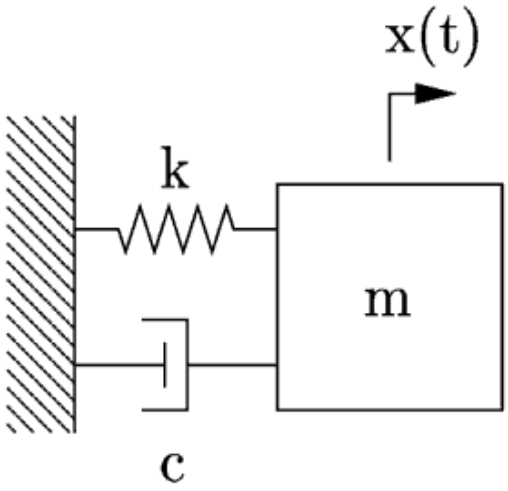

Figure 3.1. A simple grounded mass-spring-damper system.

The analytical solution to this problem is very well documented and the free response is defined by a set of equations that can be found in any basic vibrations textbook. These equations will produce a solution for the position and velocity of the mass as it responds to being released with initial position and velocity. The numerically solved response will produce an identical time series to the analytical solution, but the problem setup can use either MATLAB or Simulink. When coded into MATLAB, the ordinary differential equation solver *ode45* is used. This function iteratively observes the state trajectories and adjusts the states as necessary for the following time-step. The code used to solve the response of the simple MSD system can be seen in Figure 3.2.

```
m = 1;                  %  mass of the system in meter
k = 50;                 %  stiffness of the spring (N/m)
c = 20;                 %  damping coefficient
wn = sqrt(k/m);           %  natural frequency (rad/sec)
zeta = c/(2*wn*m)           %  viscous damping factor
 x_0 = 1;                %  initial displacement
x_dot_0 = 0;              %  initial velocity
X_0 = [x_0,x_dot_0];        %  form a vector(array) of initial conditions
tol = 1e-6;             %  tolerance of error for ODE45 solver

%function
[t,y] = ode45('pmsd_sol',0,t_final,X_0,tol);
 x = y(:,1);             %  displacement x(t)
x_dot  = y(:,2);          %  velocity x_dot(t)
yd1 = y(2);
yd2 = -(k*y(1)+c*y(2))/m;
ydot = [yd1;yd2];
```

Figure 3.2. Representation of the MATLAB code used to solve the MSD system.

This process is simplified slightly when using Simulink because the original EOM of equation (3-1) can be used. To mimic the differential EOM a series of integrators and feedback loops are utilized. As can be seen in Figure 3.3, gain blocks are then inserted to multiply the parameters of the system by the position, velocity or acceleration as required to create the original EOM.

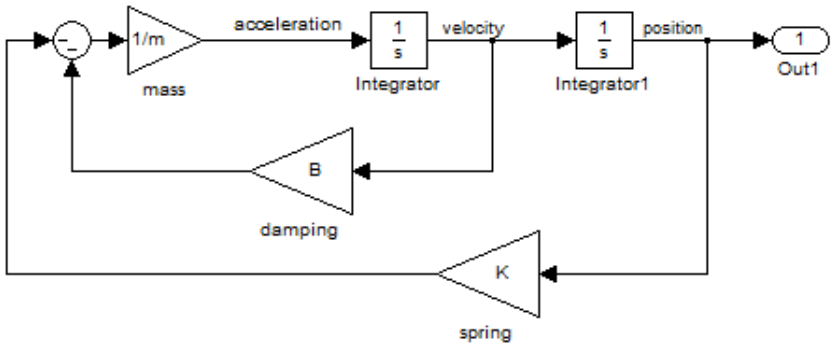

Figure 3.3. Representation of the Simulink code used to solve the MSD system.

Neither of the illustrations of Figure 3.2 and Figure 3.3 has a direct physical connotation to the original system. This requires the user to have a fine grasp of the techniques necessary to form and solve the differential EOM. This process appears to be very easy for the case of the simple MSD system, but increased complexity in the original system leads to amplified complexity in the process of numerical simulation.

The final method for solving for the response of this system is by the use of a multi-body dynamics simulator such as SimMechanics. Figure 3.4 shows the simple MSD system as it would appear in the SimMechanics environment. This representation retains a great deal of physical relation between the model and the original system of Figure 3.1. The properties of the mass are modeled within the *Body* block at the right, while the dynamic components (spring and damper) are defined by the *Body Spring & Damper* block. The *Prismatic* joint is attached to the *Joint Sensor*, which is used to measure particular variables in the same manner as a physical sensor would, in this case displacement and velocity of the mass with respect to the ground. These outputs can then be sent directly to the MATLAB workspace, where further analysis can be performed.

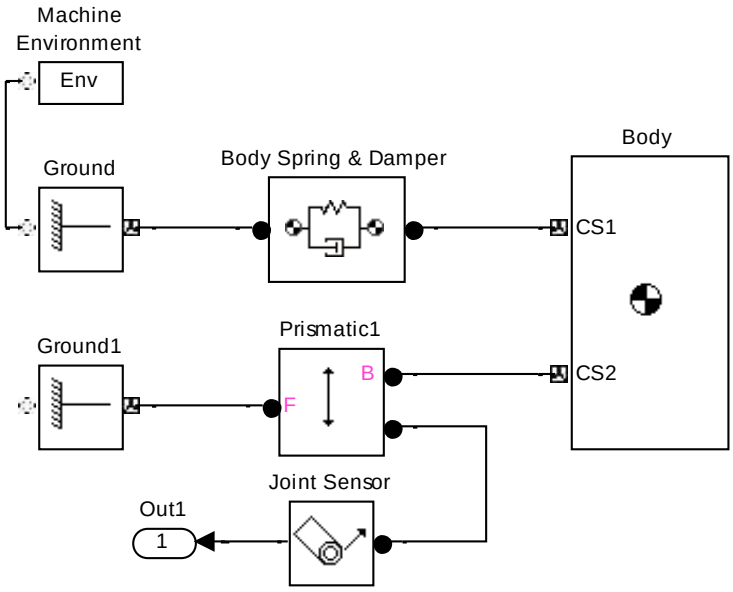

Figure 3.4. The MSD system as depicted using SimMechanics. Notice the physical nature of the modeling environment.

As has been shown, the SimMechanics environment provides a sound platform from which to build a dynamic simulation. The seamless transfer of data between SimMechanics/Simulink and MATLAB further adds to the appeal of this modeling program. Attempting to analyze a system as complex as the Proteus by use of analytical or numerical solutions would not be possible with nearly the amount of detail as is available when modeled in SimMechanics.

3.3 Proteus Modeling

The previous section described the usefulness and ease-of-modeling provided by utilizing the SimMechanics environment, but building simulations to properly represent complex physical systems is hardly as easy as it may seem. For this analysis, the concept of a four-post shaker rig was borrowed from the automotive suspension design field and applied to the Proteus in a virtual environment. Figure 3.5 and Figure 3.6 depict the testing portion and driving components, respectively, of the shaker rig located at the VIPER facility in Danville, VA. It can be seen that large pistons are used to drive pads supporting each tire, allowing for realistic terrain inputs to be

applied in a controlled laboratory setting. A virtual four-post rig was chosen as the basis for the Proteus modeling because it allows for proper excitation of the vessel with respect to the front- and side-views, while keeping it steady in the top-view.

Figure 3.5. A stock car rests atop the input pads at the shaker rig located at VIPER in Danville, VA. Photo by author, 2011.

Figure 3.6. The under-workings of a shaker rig involve very large numerically controlled hydraulic pistons used to excite the vehicle's suspension. Photo by author, 2011.

The model developed for the Proteus varies in one major way from the four-post rig depicted above. Instead of modeling the interaction between the ocean and pontoons, which is

the equivalent to the vertical dynamics of a tire on a car, the simulation was created as a hub-coupled model. This means that the inputs being used to excite the model are actually applied to the top of the pontoons rather than below them. By choosing to neglect the hydrodynamic effects occurring at the pontoons, several potential problems could be avoided in the simulation. The first is the difficulty of predicting inputs due to the variability of wave fields as opposed to a known roadway. The other issue stems from the complex nature of the water-pontoon interaction as opposed to the tire-road interaction. The complexity stems from the codependent relationship between water and hull: not only does the wave provide forces to the pontoon much like the roadway does to the tire, but the pontoon also physically changes the structure of the wave as it passes by, unlike a rigid road. By creating a hub-coupled model for the Proteus, all hydrodynamic effects are neglected, leaving only the structure itself to be analyzed.

One major obstacle ever-present when attempting to model a system as large and complex as Proteus is ensuring kinematic and physical precision and accuracy with respect to the actual vessel. To guarantee this, an additional Mathworks tool called SimMechanics Link was implemented and allowed for the exact translation of a properly constrained CAD model into SimMechanics. A solid 3-D CAD model was provided by MAR for use in creation of the simulation. Using Solidworks, material densities were applied to each part and custom translational joints appearing like shock absorbers were designed to mimic the springs for ease of force application in the dynamic model. Each individual constraint between vessel components was then analyzed to ensure proper kinematics were transferred to SimMechanics and that no individual parts, no matter how small, were left underconstrained. Figure 3.7 depicts the front and rear suspensions as modeled in Solidworks.

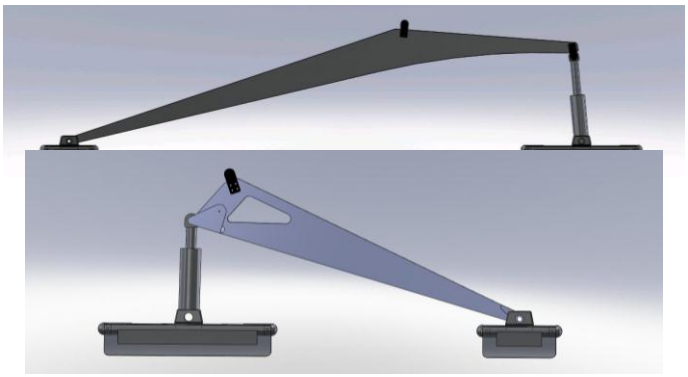

Figure 3.7. Leaf springs were replaced with cylinders to ease the process of dynamic force application within the SimMechanics environment. Top: front suspension / Bottom: rear suspension.

Due to the physically oriented nature of the SimMechanics programming environment, an emphasis was placed on organizing the model to mimic the top-view of the Proteus. A comparison between the SimMechanics and Solidworks models can be seen in Figure 3.8 below. In the block diagram at the top of this figure the orange block and green blocks contain subsystems with the driver model and suspension models, respectively. Each of the grey blocks contains the physical information for a portion of the sprung mass (including total mass, rotational inertia and center of gravity location) and the blue blocks represent joints with defined degrees of freedom. The joints connected to each suspension subsystem represent the revolute joints (1 rotational DOF) atop the suspension rocker arms and the joint at the center of the diagram represents the main spherical joint between the front arch and cabin.

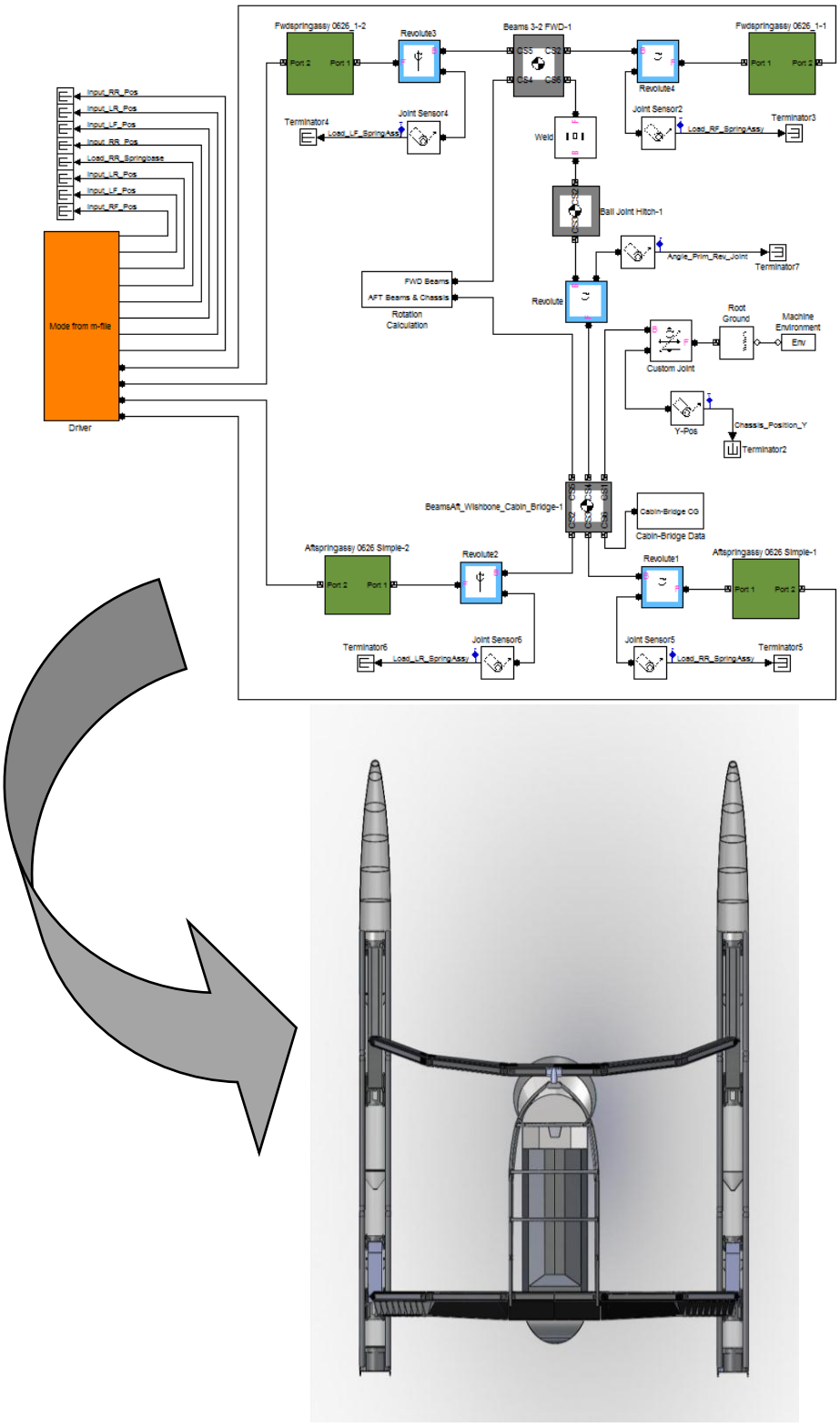

Figure 3.8. The SimMechanics model was organized to be visually comparable to the Proteus top-view appearance.

Due to the nature of using a spherical joint between the front arch and cabin, the pontoons are forced to be in tension at all times. This makes them a major component in the primary structure of the system. For this study it was important to ensure that the pontoon dynamics did not make a considerable effect on the response of the vessel, thus the spherical joint present on the Proteus was replaced with a revolute joint rotating about a longitudinal axis. This replaced the tension in the pontoons with a bending moment supported at the primary joint.

Creating forces from dynamic components in SimMechanics can be accomplished in a variety of ways. In this study a high degree of customization was desired from these elements due to the inherently nonlinear nature of the Proteus suspension configuration. For this reason, the spring and damper forces were created by applying a force along the line of action of the translational joint which was calculated as a function of displacement and velocity. This allowed for the application of nonlinearities, bump and rebound stops, asymmetries and nearly any other suspension abnormality imaginable. The constraints applied to the suspension bases restricted them from rotating in pitch and allowed for vertical translations to be the driving motion while leaving the other four DOF free to move. These DOF are described with arrows in Figure 3.9, where blue indicates freedom of motion and red indicates the driver.

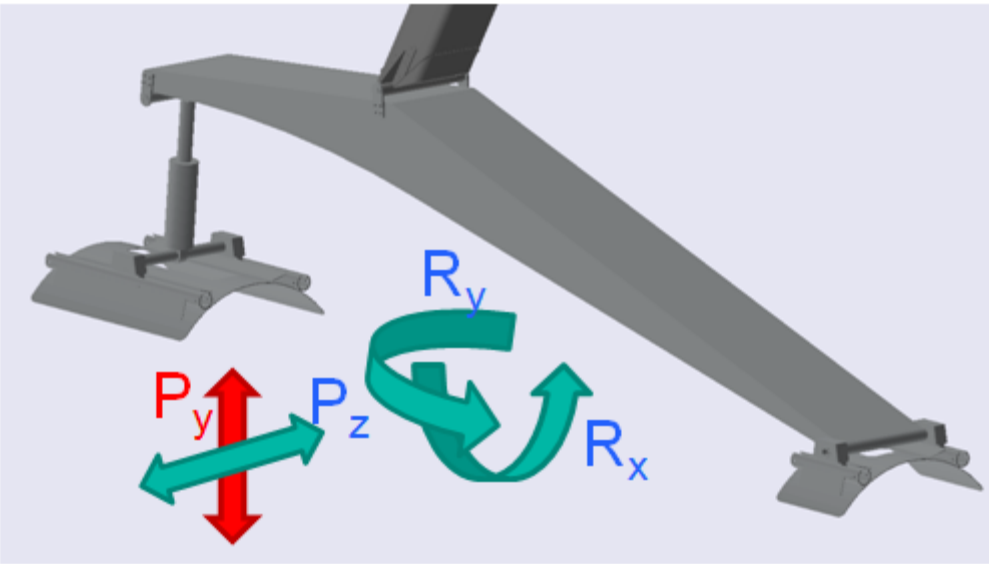

Figure 3.9. The suspension bases were only restricted from pitching rotations and were driven with vertical translations. Here the capital letters P and R stand prismatic and rotational axes, respectively.

These constraints alone, however, are not enough to ensure that the vessel does not encounter rigid body motion (RBM) during simulation. In order to keep the entire Proteus model steady, a set of constraints was also applied to the CG in the cabin mass block. These constraints only allow the chassis to translate vertically and exhibit roll and pitch rotations. This ensures that the entire model does not drift away in either direction of the top view or yaw, either of which could cause solution errors or simulation crashes.

SimMechanics allows for a model to be excited in one of two ways: via translations and rotations, or forces and torques. The latter is very useful when the exterior connections to the physical model are dynamic in nature or are defined by force interactions. Excitation by motions, however, is much more suitable for this study because the dynamic nature of the pontoon-water interaction is being neglected. The use of motion as the driving element leads to a complication in SimMechanics, however, because this motion must be described by a three-component signal: displacement, velocity and acceleration. Therefore, the model designer must calculate derivatives, integrals or both depending on what form the motion was originally defined in. The most obvious method comes from using derivative or integral Simulink blocks to perform the required tasks. These, however, come at the downfall of potential inaccuracies or instabilities depending upon the original signal (especially if these signals contain discontinuities). A second method exists which utilizes transfer function blocks to perform these tasks. This offers the user a method of not only performing the required calculations, but also applying filtering or smoothing schemes before or afterwards. The final method is to numerically calculate the three components of the motion signal using MATLAB before they are even sent to the simulation. This pre-processing method has shown the most consistent results throughout the study and was utilized for each ensuing model.

3.4 Parametric Analysis

To investigate the potential effects of various changes to the original configuration of Proteus a parametric analysis was planned and executed on the SimMechanics model discussed previously. Before performing this study, however, proper inputs had to be created which could be used to

thoroughly understand the effects of parameter changes. Real oceanic inputs were not available for this vessel, so a simpler input model had to be created. It was decided that a continuous harmonic signal would be utilized, such as a sine-wave. If, however, a simple sine was applied as a displacement input it would result in a discontinuous startup value for the velocity. This is shown in equations for position, velocity and initial velocity of (3-2), (3-3) , and (3-4) below.

$$y(t) = A\sin(\omega t + \phi) \tag{3-2}$$

$$\dot{y}(t) = \omega A\cos(\omega t + \phi) \tag{3-3}$$

$$\dot{y}(0) = \omega A\cos(0) = \omega A \tag{3-4}$$

The initial velocity seen in equation (3-4) is analytically equivalent to superimposing an impulse force at each of the four inputs at model startup. To remove this discontinuity, a new input method was derived and is described in equations (3-5), (3-6), and (3-7).

$$y(t) = A - A\cos(\omega t - \phi) \tag{3-5}$$

$$\dot{y}(t) = -A\omega\sin(\omega t - \phi) \tag{3-6}$$

$$y(0) = \dot{y}(0) = 0 \tag{3-7}$$

In an effort to simulate various potential effects of different incident angles of wave impact to the vessel, four modes of input motion were used in this study including heave, pitch, roll, and warp. Heave occurs when each input is identical at all times, creating a purely vertical excitation. Pitch and roll inputs are used to excite the vessel in a rotational sense about the lateral and longitudinal axes, respectively. Warp inputs involve exciting the vessel in such a manner as to twist it about its longitudinal axis. Creating these inputs only requires the proper application of two signals, one lagging the original by 180 degrees, but identical in every other parameter as can be seen in Figure 3.10. By supplying each corner with the proper input signal, each of the four modes can be created. Table 3-1 summarizes these modes of motion and the lead/lag of the signals to each corner required to create them.

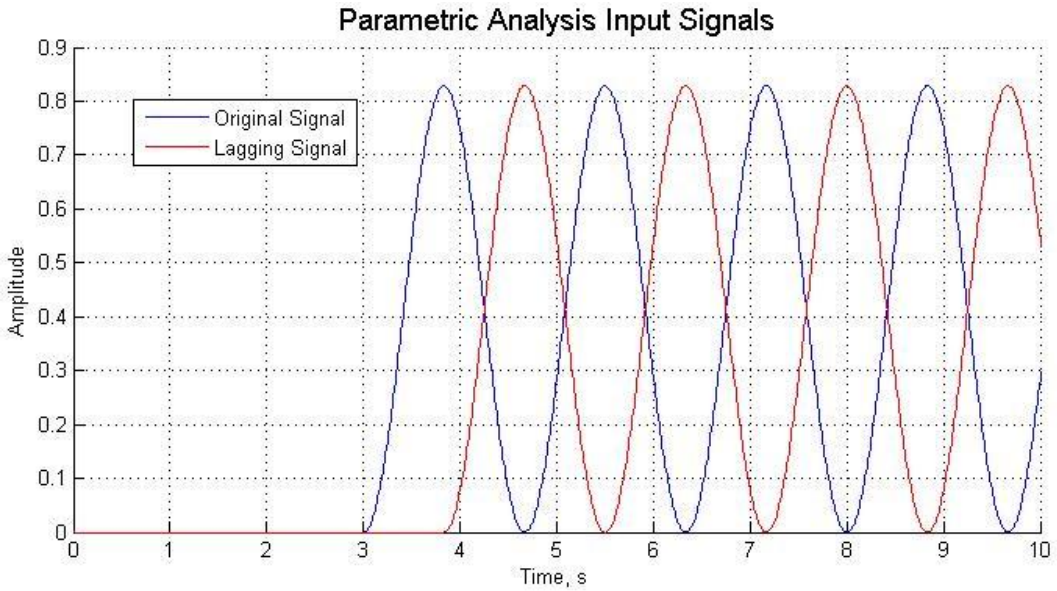

Figure 3.10. The signal used to drive the parametric model removed as many discontinuities as possible.

Table 3-1

Description of Modes of Input Motion to Proteus

Motion	Description	Phase Lag (deg)			
		LF	RF	LR	RR
Heave	Vertical bouncing	0	0	0	0
Pitch	Rotation about lateral axis	0	0	180	180
Roll	Rotation about longitudinal axis	0	180	0	180
Warp	Combination of Roll and Pitch	0	180	180	0

Parametric studies are used to observe the behavior of any system with respect to the variation of particular interesting parameters. The goal of the study is to summarize the effect of the variation of these parameters on some quantifiable output metric which reasonably describes the vehicles behavior and rate them on the basis of their sensitivity. Sensitivity as defined in equation (3-8) can represent either a direct $(+)$ or inverse relationship $(-)$, with the final parameter ranking being based upon absolute sensitivity.

$$Sensitivity = \frac{\%\ \text{Change in Output}}{\%\ \text{Change in Parameter}} \times 100 \tag{3-8}$$

In an effort to keep the study as simple as possible the number of output sensors had to be limited. The most important response for analyzing the effects of suspension alterations is the vertical acceleration on the chassis. This should be directly indicative of the ability of the suspension to mitigate wave inputs to the payload and cabin. It was also desired to investigate the suspension effects on the longitudinal acceleration. This came about in an effort to discover the root cause of a particular lurching motion felt at the cabin. Reports coming from those who have gone underway in Proteus claim that a strong longitudinal oscillation can be felt in the cabin as the vessel passes through waves.

This longitudinal dynamic study, however, was limited due to the constraints applied to the model as described near the end of Section 3.3 above. In order to restrain the entire system from drifting laterally or longitudinally during simulation the cabin was pinned from any motion in these directions. Other methods were tested to properly constrain the model without directly limiting the motion of the chassis, but each resulted in side-effects which caused binding and bogus simulation outputs and therefore could not be used. For this reason, any longitudinal motion of a sensor upon the chassis would be a direct result of a kinematic relationship to the pin joint at the cabin CG. Therefore, in order to fulfill the purpose of this study, only the vertical chassis acceleration would be used to analyze the parameter sensitivities.

Due to the time-varying nature of this output signal, a set of statistical values was chosen to summarize it. For this analysis the maximum, minimum, inter-quartile range and root mean square were used. It should be noted that the each cabin acceleration dataset was detrended to zero-mean; indicating that the minimum represents the maximum negative acceleration and the root mean square is mathematically equivalent to the standard deviation. The chosen parameters and their percentage variations are represented in Table 3-2. As the reader may notice each parameter is varied symmetrically in the positive and negative directions with the exception of the sprung mass, which has an extra data point at +75%. This was done because the Proteus baseline model much more closely reflected a light cargo payload. In order to quantify the percent variation in CG position, baseline values had to be defined for relating the changes to.

Longitudinal CG variation was calculated as the percentage displacement of the CG with respect to the vessels wheelbase (longitudinal distance between front and rear arch attachments to springs) while the vertical CG variation relies upon the motion relative to the baseline static CG height as measured from the top of the pontoons.

Table 3-2

Percent Variation of Parameters

Parameter	% Variations
F & R Spring Rate	± 25%, ± 50%
F & R Damper Coeff.	± 25%, ± 50%
Sprung Mass	± 25%, ± 50%, + 75%
CG Longitudinal	± 10%, ± 20%
CG Vertical	± 22%, ± 44%

The results of each test were then compiled into spreadsheets for further summarization and analysis. The major obstacle encountered at this stage was the sheer amount of data available even with a minimized set of parameters and only a single output. The information presented in Table 3-3 depicts an example of the sensitivity results of just two parameters being varied four times from baseline for only a single excitation mode. In order to present the parametric sensitivities of the Proteus in a practical manner, each of these sixteen-value arrays had to be summarized by as few characteristics as possible.

Table 3-3

Example of Sensitivity Results

		Parameter Sensitivity (%)			
		Max	Min	IQR	STD
F. Spring	-50% F. Spring	-12.36	17.12	-15.27	-14.36
	-25% F. Spring	-12.19	66.39	-13.27	-11.91
	+25% F. Spring	-6.79	-154.31	-5.99	-9.65
	+50% F. Spring	-5.59	35.83	-6.67	-6.84
R. Spring	-50% R. Spring	-2.15	-20.12	-1.99	-1.65
	-25% R. Spring	-3.53	146.07	-4.37	-1.60
	+25% R. Spring	-0.80	-149.56	-3.56	-3.26
	+50% R. Spring	-1.08	-10.74	-1.70	-1.89

When beginning to analyze the data it was found that the most consistent sensitivity results came from the inter-quartile range and standard deviation statistics of the time-series output data. Transient data near the beginning of each simulation sometimes led to outliers being

recorded as the maximum and minimum values which then created misleading sensitivities. The standard deviation also represents some of this outlying data, but the inter-quartile range is a robust statistic and is immune to its effects. Both of the latter statistics, however, display good capabilities summarizing the changes in the oscillating amplitude between signals.

It can be seen in Table 3-3 that the output sensitivities for every statistic vary down each column with the alteration of the parameter values. It was desired that the amount of sensitivity and variance of that sensitivity be captured for the subset of data including the inter-quartile range and standard deviation. This results in only two values for each parameter and excitation direction which can be used to describe the output sensitivity. Taking the mean of these sensitivity arrays provides an average sensitivity for each parameter and can be used to rank parameters. The variance (in this case defined by the standard deviation) can be used firstly to see how much the sensitivity varies as the parameter is changed and secondly to identify potentially faulty data which is often the result of low baselines.

It was also desired that the vertical acceleration output measurements be investigated for variance with changes in sensor location from the aft end of the payload forward to the cabin. This could be important information for any variant of the Proteus involving sensitive payload or passengers spread throughout the payload space. Three sensor locations were chosen with respect to the arch attachments at the front and rear suspensions: 80% forward, mid-span, and 80% rear. This allowed for a brief but informative investigation into the trends associated with longitudinal position within the vessel.

One major downfall haunts the aforementioned method of output sensitivity analysis which is low baseline output values because they tend to provide larger percentage changes in output values with the same parameter variations. When these baseline values fall too low, the mean sensitivity values tend to raise considerably, but so do also the variances of these sensitivity measures. All of this leads to data that cannot but supported for further analysis into the study and therefore must be neglected. One idea to consider, however, is that any low baselines are indicative of a lack of excitation in the direction of consideration at the payload and that neglecting them is completely acceptable. Several sets of data fell into this range of unsuitability and were discarded. For the vertical accelerometer only the heave and pitch

excitations showed promising response, with roll and warp producing little cabin motion. These low baselines led to wildly variant sensitivities with amplified means, which makes sense because the roll and warp inputs would likely produce very small vertical oscillations at the chassis.

The results from the heave excitation show clear sensitivity trends and are probably the best indicator of the parametric variation capabilities of the Proteus suspension system. Figure 3.11 displays this result where each set of bars symbolizes a different parameter and, as the legend indicates, the blue bars are for the front sensor, red for the middle sensor, and green for the rear sensor. It should be noted that the zero-sensitivity mark is denoted with a horizontal line; anything above it corresponds to a direct relationship and anything below represents the inverse. In this figure the parameters of front and rear damping rate and CG vertical position were left out because their sensitivities were negligible as compared to the others.

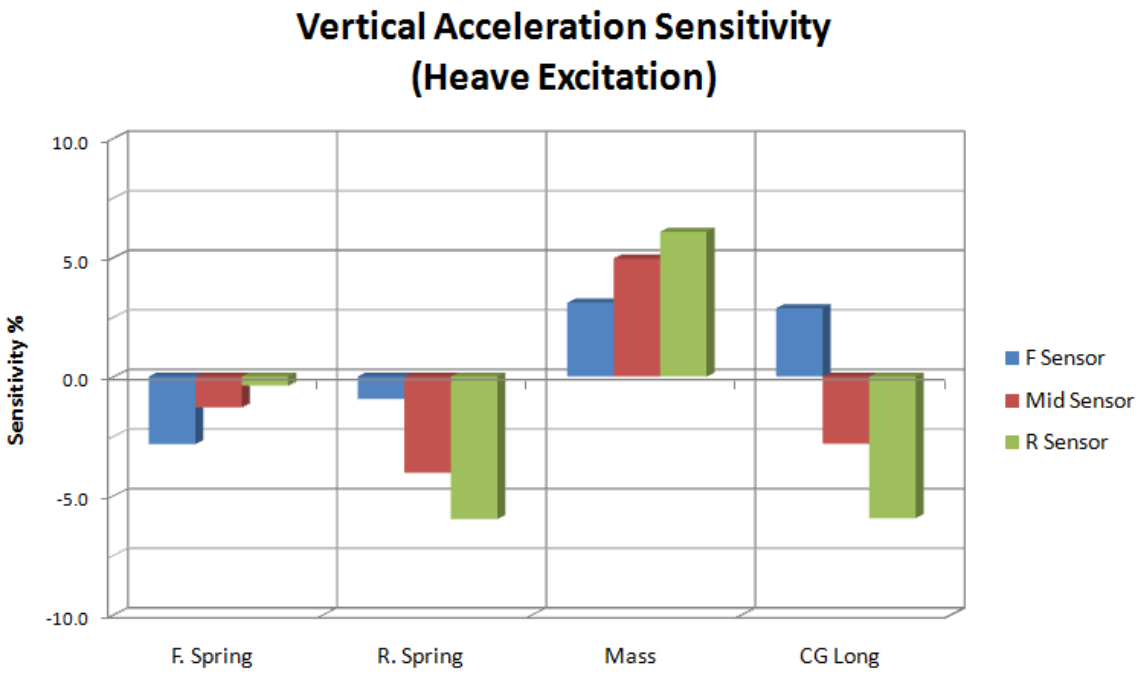

Figure 3.11. Variance in output sensitivity percentage from front to rear of the chassis from heave input.

The first trends of note are the front and rear spring rates, which offer opposite and nearly equal trends. As can be seen, both curves are completely contained within the inverse relation side of the axis and increased absolute sensitivity to either spring is felt at a sensor position closer to that suspension. The mass parameter, on the other hand, shows a direct relationship

with increased sensitivity as the sensor is moved rearward. For this particular model the rearmost sensor was the closest to the baseline CG which could indicate why the sensitivity tends to increase as the sensor approaches its aft location. The longitudinal position of the sprung CG also played a major role in the vessel dynamics. At the rear and central sensors an inverse relationship exists where any forward translation of the mass results in a decrease in sensed acceleration. The forward sensor, however, revealed the opposite effect, where forward motion results in an increased acceleration.

When the vessel was excited in pitch the vertical acceleration oscillations held a much lower baseline than in heave. This effect was pronounced at the central sensor position where the baselines accelerations fell to approximately twenty percent of what was shown at the front and rear. It is believed that this effect comes as a consequence of the kinematics involved in exciting it in this manner. As the sensor approaches the center of the wheelbase it also approaches the pitch center of the input resulting in minimal vertical motion. This led to elevated sensitivities at that sensor location as well as increased variation across parameter changes. For this reason only the front and rear sensors were evaluated for sensitivity resulting from pitch input.

When analyzing the results from pitch excitement, there are many similarities to the heave data, but there are also a few particular differences. The primary similarity between the pitch excitation data of Figure 3.12 and the corresponding data presented above from heave excitation in Figure 3.11 is that each parameter shows an identical trend direction from both excitations with the exception of the vertical CG position which was omitted from the prior analysis due to low sensitivity values. Furthermore, the sprung mass and front and rear spring rates showed nearly identical data in both studies. The most obvious difference between the two studies is the longitudinal CG position. In the case of pitch excitation, this parameter plays a very overbearing role at the rear sensor, but it's important to note the potential root cause of this outcome. When the CG is moved forward from its baseline position it gets closer to the pitch center of the excitation drivers, which indicates that the sprung mass will then receive a reduction in vertical input motion. Since the vertical input is actually being reduced in this case, it makes sense that a high sensitivity would result. It is believed that this phenomenon shows its effects to a greater extent at the rear sensor because it is so much closer to the baseline CG

position. The similarities in the results present between the heave and pitch input modes can be attributed to the coupling effect which comes about due to the WAM-V™ geometry. The sprung mass CG of the Proteus model is well aft of the midpoint between the arches in the side view. This means that as the vessel is excited in pitch, the sprung mass CG encounters a lot of vertical motion just as it would from the heave input. A sprung mass pitching response could potentially be forming from pure vertical excitation due to stiffness differences of the front and rear suspension as well as the rear weight distribution of the sprung mass.

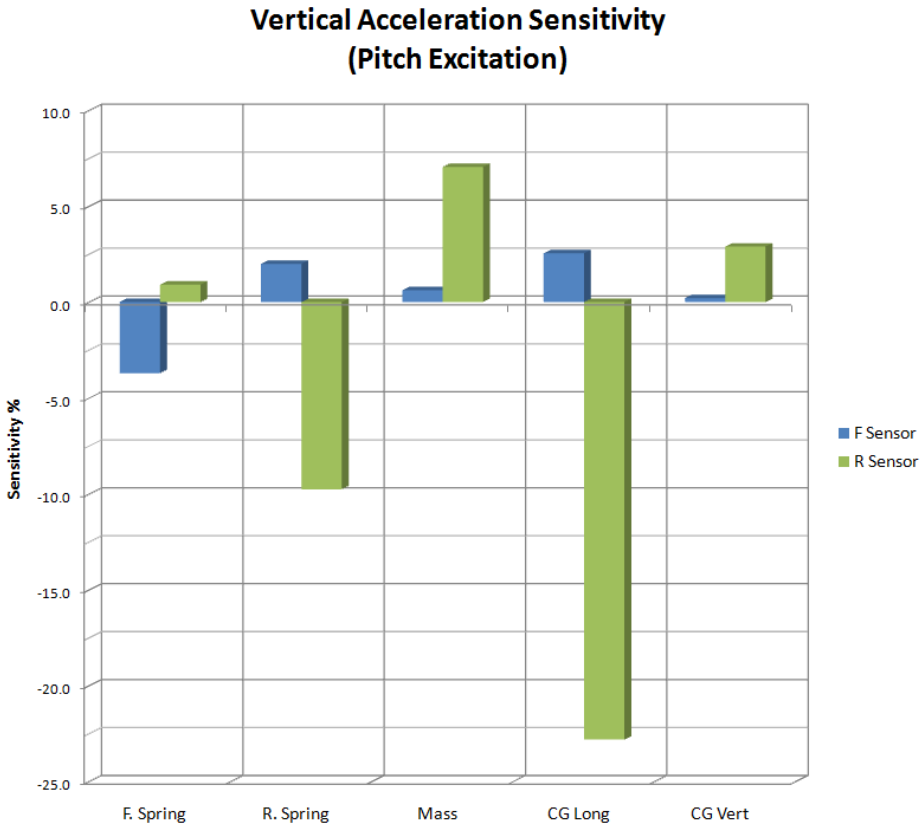

Figure 3.12. Variances in output sensitivity from front to rear of the chassis from pitch input.

In conclusion, it has been shown that repeatable trends can be derived from variations in parameters under different excitation conditions. Both suspension spring rates seemed to make an effect on vertical cabin acceleration, with each playing a greater role on its respective end of the payload and an increased absolute sensitivity for the spring closer to the sprung mass CG location. These results seem to indicate that an increase in suspension stiffness should result in an overall reduction in chassis accelerations. The sprung mass and location of that mass also

played a role in the response of the system, with greater absolute sensitivity occurring at sensor locations closest to the sprung mass CG. The total sprung mass seemed to have an effect of increased chassis acceleration with an increase in mass. Varying the location of the sprung mass CG indicated that decreases in cabin acceleration could be accomplished with a lower CG that is closer to the center of the wheelbase longitudinally.

Chapter 4

Unmanned Surface Vessel Characteristics

Future interests with WAM-Vs™ lay in smaller vessels that can be operated remotely and/or autonomously. One such vessel, developed by MAR, was made available to this study for static and dynamic testing. The purpose of this chapter is to discuss the process of creating a dynamic model for this unmanned surface vessel (USV). The USV design is laid out and compared with Proteus to highlight any differences in their basic architecture. The methods used to gather the required physical properties are covered followed by a presentation of the model developed to mimic the USV response. The final and most important section details the processes used and results of the interpretation and estimation of the spring and damping rates applied to the model.

4.1 USV Design Overview

The USV design is very similar in architecture and kinematics to its predecessor Proteus. However, after observing substantial flexing of the pontoons on Proteus during open-water testing, it was decided by the designers to affix rigid skis between the front suspension and the rear arch attachment atop the pontoons of the USV. These skis offer multiple benefits by providing a stable platform to build the suspensions atop of and preventing the difficult-to-understand flexing of the pontoons. Figure 4.1 shows the USV configuration along with callouts to define the nomenclature of each individual component. From this image it can be seen that the USV retains several aspects of the Proteus design including a rigid connection between the rear arch and the payload tray as well as a spherical joint between the payload tray and front arch, allowing the front of each pontoon to move independently.

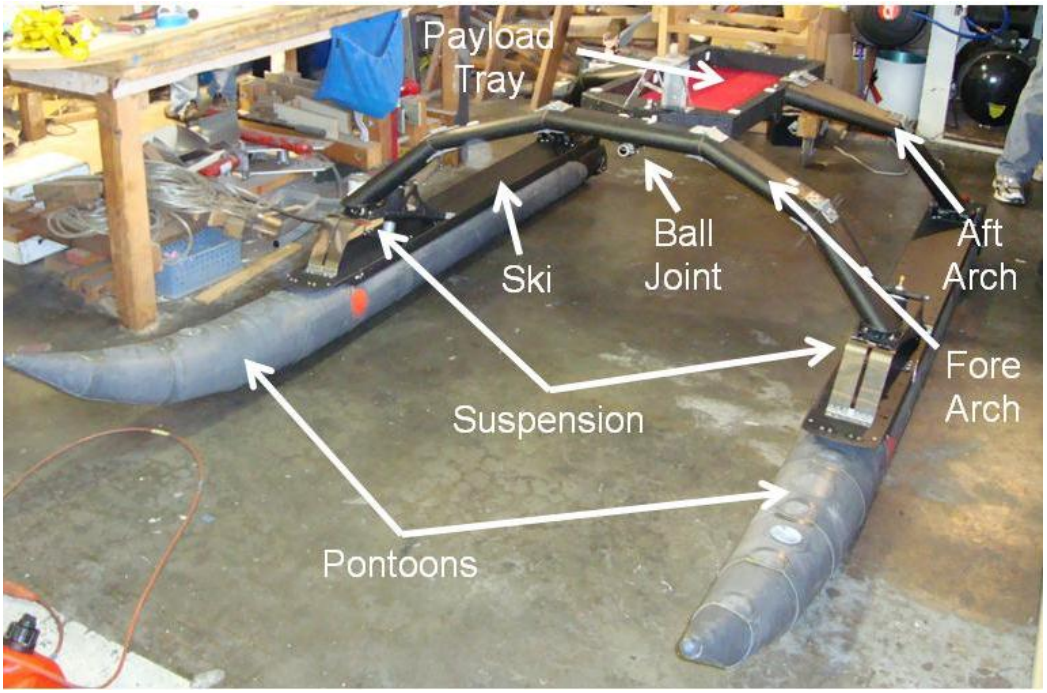

Figure 4.1. The USV retains representative architecture to Proteus with the obvious addition of rigid skis between the front suspension and rear arch attachment. Photo by author, 2011.

In light of the relative stiffening of the pontoons offered by the addition of skis, two major kinematic alterations had to be made to the original Proteus design to allow for properly constrained motion of the pontoons. At the connection between the rear arch and the pontoon a custom two degree-of-freedom joint was created. This connection is fashioned by passing a plastic shaft through a conventional ball-and-socket arrangement and constraining its end points to only move longitudinally as can be seen in the images of Figure 4.2 below. This joint differs greatly from its counterpart on the Proteus because it allows for the direct transmission of input forces to the cabin via the rear arch rather than conveying them through a suspension system.

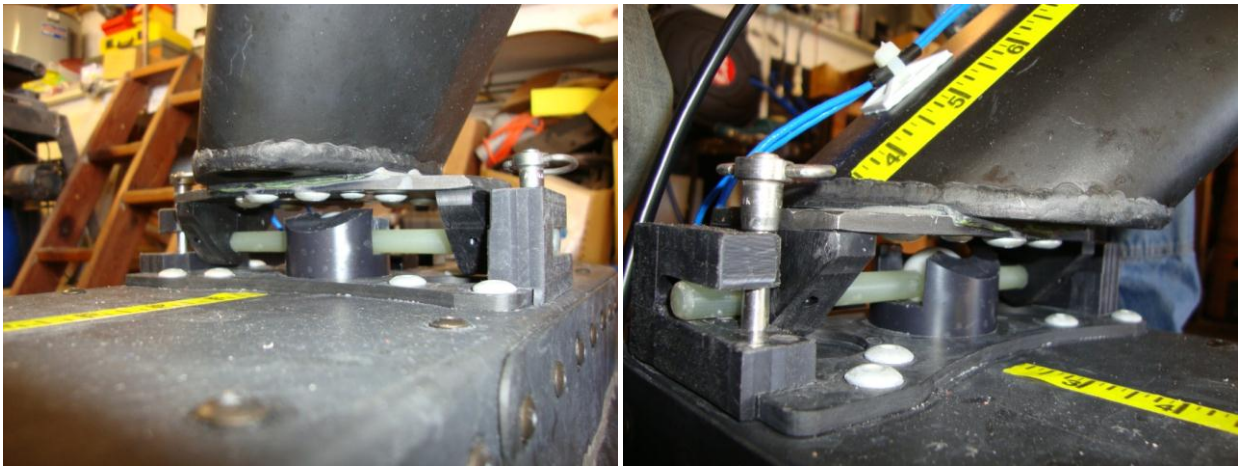

Figure 4.2. The rear joint of the USV utilizes a combined ball and shaft to allow it freedom to rotate about the transverse and vertical axes only. Photo by author, 2011.

Another alteration to the basic Proteus configuration is the use of a spherical joint between the front arch and the front suspension. As can be viewed in the callout of Figure 4.3, this joint, along with its counterpart in the rear, allows for the proper motion of the pontoons with relation to one another. From this image, the reader may notice that the suspension of the USV is also slightly altered from the original Proteus design. Rather than relying solely on leaf springs to supply the elastic force, a gas spring was installed to produce the majority of the returning force of the suspension system.

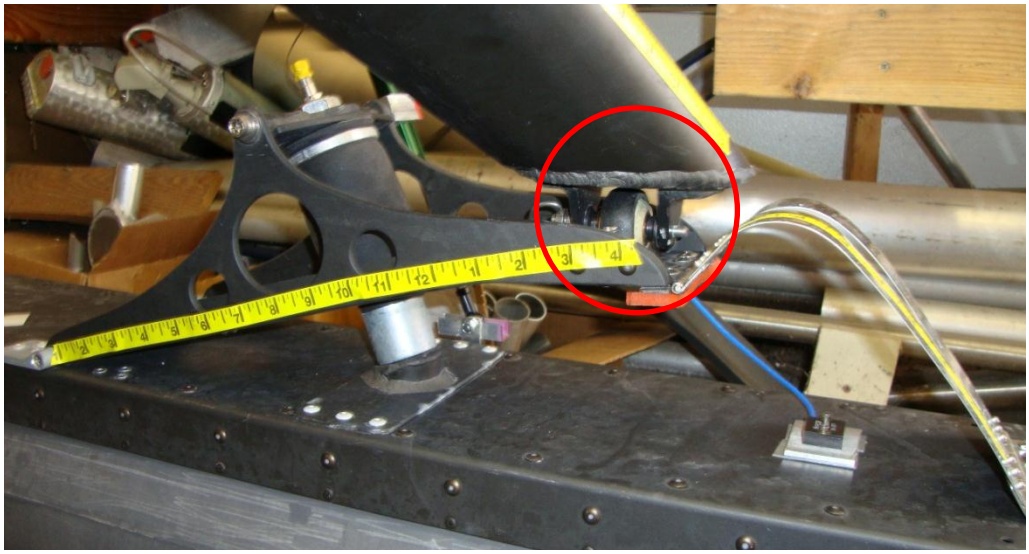

Figure 4.3. A spherical joint was utilized to attach the front arch and suspension and to allow for properly constrained motion of the pontoons relative to one another. Photo by author, 2011.

4.2 Physical Property Measurement and Static Testing

In order to create a representative multi-body dynamic model of the USV, particular parameters had to be measured as accurately as possible. The most important physical parameters of interest were the weights of each component and the location of that weight. Individual components are easy to weigh with a small scale after disassembly, but locating that weight with individual centers of mass can be a time-consuming and difficult task. For this reason, the longitudinal center of gravity (CG) of the entire vessel without engine pods, electronic receivers or a payload was found by balancing the vessel atop a piece of two-inch diameter tubing long enough to support both pontoons simultaneously. Particular attention was then paid to the position of the removed components, especially the CG of the engine pods and the geometry and position of the fuel tank within those pods. With this information along with the mass and shape of each component on the vessel, individual CG's could be estimated using a three-dimensional CAD model with distributed masses. Individual mass moments of inertia were not measured directly on the vessel and therefore had to be estimated as will be discussed in the following section.

The next and potentially most important step was to measure the spring rate of the suspension. In order to accomplish this, a scale was placed upside-down atop the payload tray and in successive steps, weight was added to the scale while measurements of the displacement of each spring were gauged using digital calipers. The raw results of this measurement and the final deduced spring force vs. displacement curves are presented in Section 4.4 below.

4.3 USV Multi-Body Dynamic Model Development

Although the USV and Proteus are very similar in architecture, a much different approach had to be taken when creating this multi-body dynamics model. A detailed 3D CAD model was not available for this portion of the study, so one had to be constructed from measurements and images of the USV. This model, which can be seen in Figure 4.4, is kinematically accurate but is not physically detailed. The major downfall of this simplification is that the mass distribution – CG location and inertia tensor – of individual parts may not be entirely accurate even when their

density is varied to match the mass measurements taken when the vessel was disassembled. This could produce erroneous results due to improper physical variables in the simulation equations of motion. However these errors will be minute and negligible because the most important dimensions have remained accurate and the primary directions of rotation retain the best polar inertia information.

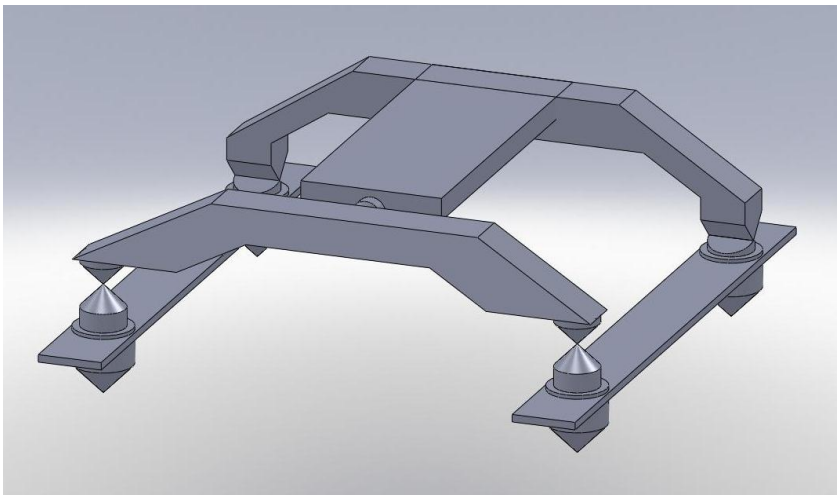

Figure 4.4. The USV CAD model is much simpler in architecture than the Proteus model.

From this depiction of the model the reader should first notice the rigid skis attaching the front and rear arches on either side. These are acting as the base for the inputs applied to the model because the pontoon hydrodynamics are being ignored as they were in the Proteus model. At the connection of the rear arch and skis a two-DOF joint was created by connecting two revolute joints together orthogonally to one another. At the front of each ski a large cylinder replaces the suspension system with a spherical joint used to connect it to the front arch. Between the front arch and payload tray a spherical joint was used to match the kinematics on the actual vessel.

The four upside-down cones below the skis represent the points of excitation input into the model. These points were left fully free to translate and rotate in space because they are kinematically constrained to the rest of the vessel. Input motions were applied in the vertical direction at each of these connections. The center of gravity on the payload tray was constrained in the same manner as the Proteus model so that it was only allowed to translate vertically and

rotate in roll and pitch. The other three degrees of freedom were fixed to ensure the entire vessel did not drift in space.

4.4 Spring and Damper Modeling

The first step toward modeling the dynamic components of the USV was to analyze and make necessary adjustments to the measured spring force data. In this measurement, a vertical force was incrementally increased upon the payload tray and measurements of spring displacement were taken with digital calipers on either side, as discussed above. To begin, the raw deflection measurements were offset such that their zeros matched then they were averaged to produce a single spring deflection measurement for each weight. The raw spring deflection vs. total force curve can be seen in Figure 4.5 below.

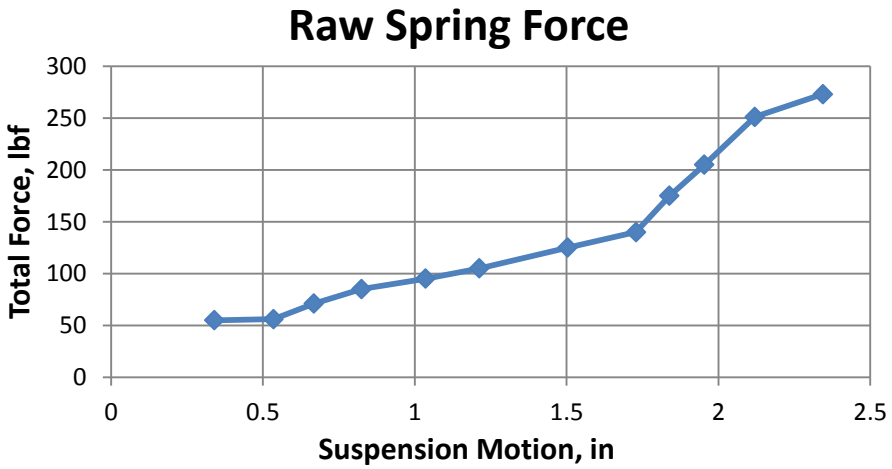

Figure 4.5. This graph depicts the averaged left and right side raw spring force data.

The reader may notice a number of non-linearities present in this force vs. displacement data. Although the presence of non-linear properties in suspension systems is very common, the root cause of them on the USV is fairly clear. In Figure 4.6 the reader will notice a view of the left front suspension system on the USV as depicted from the right side. At the top right it is clear that within a small margin of suspension deflection, the forward facing edge of the front arch will contact the leaf spring, thus causing it to deform unnaturally from its configuration. The second possible cause can be seen more centrally in the figure and stems from the rigid

connection of the bottom of the air spring to the ski. This welded joint completely fixes the air spring from rotating, which is required of this kinematic configuration.

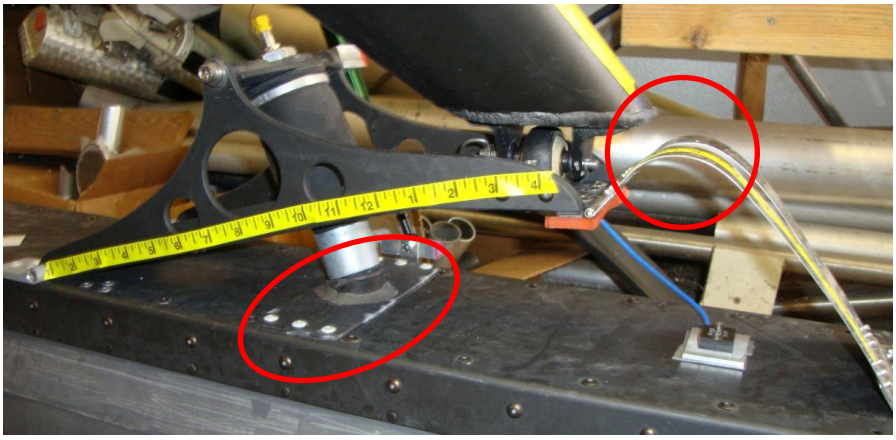

Figure 4.6. Non-linearities in the suspension stiffness arise from two major areas which are called out in this depiction of the left from suspension system on the USV. Photo by author, 2011.

Through analysis of the USV kinematics, this spring deflection was then converted to a measure of the deflection at the tip of the suspension rocker where the front arches attach. This particular displacement is required for the USV dynamic model because of the method in which the kinematic suspension constraint was simplified. The final step of the spring modeling process involves the addition of mock bump and rebound stops. The experiment to measure the USV spring rate was limited in several ways because data points could not be recorded at zero spring force due to the static weight of the structure nor completely down to the bump stops due to limited ballast sources. The effects present at these displacement locations were understood from experience and were estimated by increasing the slope of the curve at either end as can be seen in Figure 4.7. In this graphic, the blue points represent measured data and the red points at either end represent the estimated bump/rebound stop data.

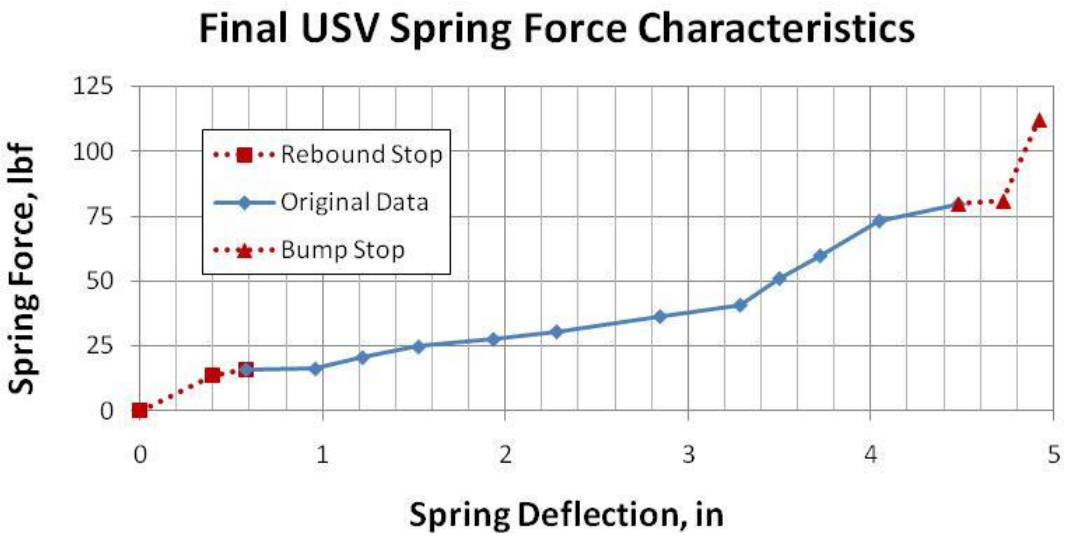

Figure 4.7. This figure represents the final single spring force vs. displacement curve. The blue points represent measured data and the red points at either end represent estimated data.

The distinct discontinuities created by this bi-linear stiffness at either end of the suspension travel could potentially lead to errors from inaccurate estimation or instabilities in the simulation solution. The bi-linear stiffness problem has even been known to exhibit chaotic behavior under particular conditions. This, however, should not be an issue with the simulation spring rates as modeled. The large rattle-space and relatively stiff springs ensure that these portions of the curve are rarely explored during simulation or actual operation of the vessel and the time spent around them is minimal.

During USV characterization there were not any experiments performed which were related directly to measuring or calculating the suspension coefficient of damping. The primary reason for this is because there are no independent dampers in the suspension system of the USV. The vast majority of damping must therefore be a result of non-linear friction damping occurring in the joints and gas spring. Trying to model this dynamic friction would be difficult and time consuming, so the non-linear damping effects were neglected for this analysis. From inspection of the vessel it was known that it possessed a very small damping ratio due to its slow energy dissipation in suspension oscillations. It was estimated that the system contained approximately a 10% damping ratio, which was to be applied as linear damping within the springs. This was accomplished by applying an initial compression of 2 inches to each suspension on the USV simulation and analyzing the spring oscillation response's amplitude decrement. The baseline

linear damping rate chosen was 30 $N - s/m$. Although the damping on the actual USV was certainly non-linear, this linear damping coefficient was used in the simulation for the sake of simplicity. A defense of this assumption is presented with the multi-body dynamics modeling results of section 5.6.

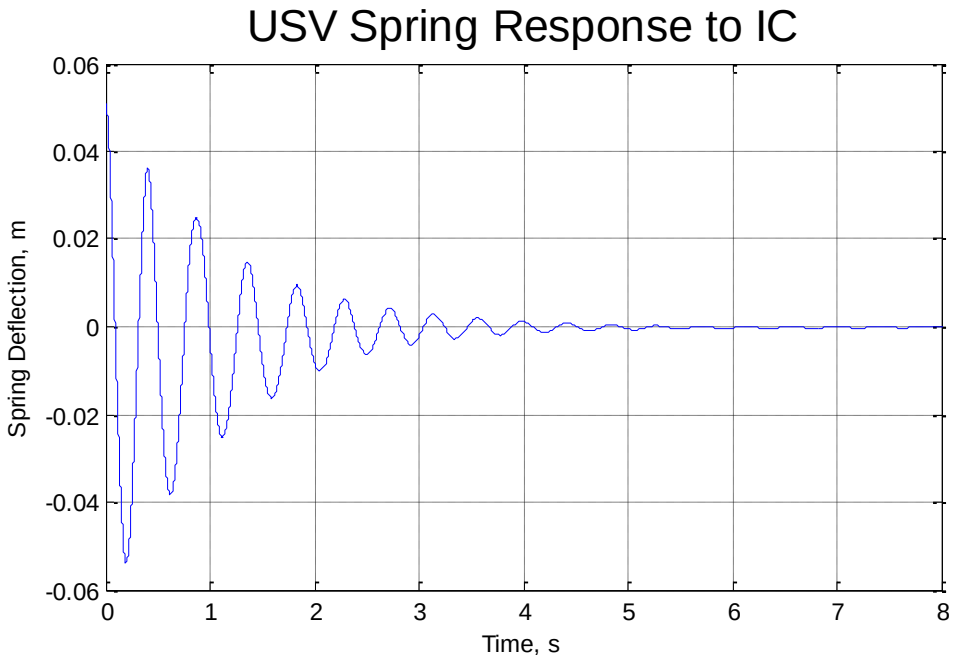

Figure 4.8. The USV response to 2 inches of initial compression exhibits the low damping ratio.

Chapter 5

Unmanned Surface Vessel Dynamic Testing

Dynamic simulations offer users the ability to avoid costly and time-consuming physical testing each time a change of system configuration requires analysis, however, these models must demonstrate their ability to replicate real systems before they can replace testing. In order to gain confidence in the validity of the dynamic models created for the USV, a set of data needed to be gathered from testing of the vessel on open water. The following chapter will highlight the acquisition of this data along with the processes involved in applying it toward model validation. After a brief discussion on USV instrumentation and test setup, the events occurring on test-day are detailed. The largest section covers the extremely important task of pre-processing the input data. A simple single degree of freedom USV model is outlined along with the analysis used to validate the usage of the measured spring force data. In conclusion, the results of the multi-body dynamic USV simulation are presented and the model's validity is defended via time-series data comparison.

5.1 Instrumentation

For the sake of versatility, a customizable data acquisition system was required for application to the test vessel. The heart of this system lies in a modular National Instruments device called the CompactRIO. The CompactRIO is a low-cost reconfigurable controller and acquisition system that combines data storage, onboard processing and swappable input/output modules. The most important attribute is its ability to run LabVIEW programs in real-time, allowing for nearly unlimited customization and data pre-processing if desired. Figure 5.1 highlights the individual components of the assembled CompactRIO system.

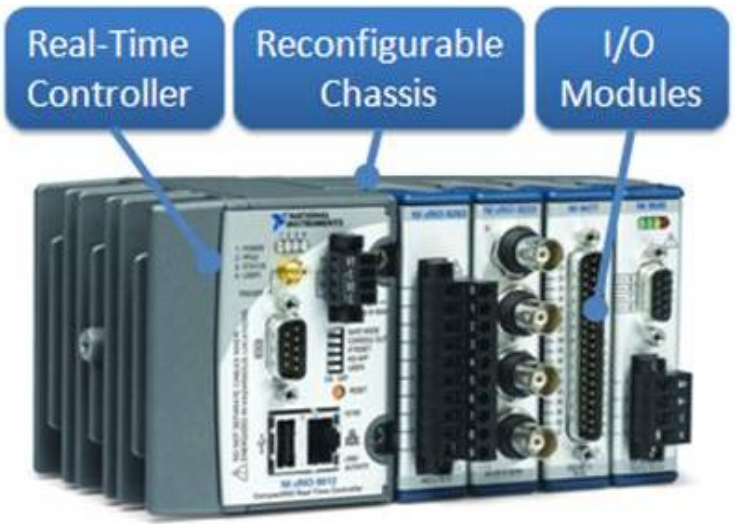

Figure 5.1. The CompactRIO is completely reconfigurable, allowing for comprehensive customization.

Although this data acquisition system is very rugged, it still required proper waterproofing to ensure nominal operation throughout the test. The CompactRIO and the 12 V battery used to power the system were affixed within a water resistant box, allowing easy access throughout instrumentation setup and testing while still ensuring proper protection for the sensitive electronics. The next issue encountered was how to pass information into and out of this box. Twelve waterproof connectors for sensors were installed into one end of the box along with an Ethernet port for connecting a computer directly to the CompactRIO with the box closed. These components can be viewed in Figure 5.2 below.

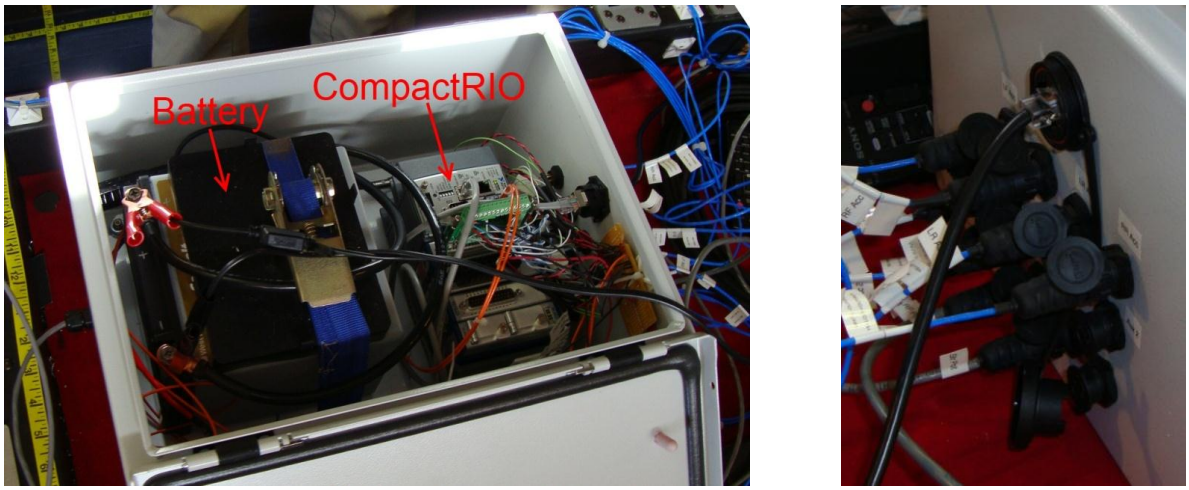

Figure 5.2. The battery and CompactRIO were situated within a water resistant box. Twelve waterproof connectors and an Ethernet port were also installed. Photo by author, 2011.

Once an acquisition system was chosen, careful attention had to be paid to sensor selection and proper installation. These sensors would be used to create the base excitations necessary for the multi-body dynamic model as well as for comparison with representative virtual sensors in the simulation for final validation. Because the model intentionally neglected pontoon hydrodynamics, it was essential that the wave inputs be recorded at points just above the pontoons. The rigid skis provided the perfect platform for this. As can be seen in Figure 5.3, the accelerometers were mounted close to each arch attachment above the skis. On the right side redundant 10g and 30g DC accelerometers were placed side-by-side to ensure that acceleration inputs over 10-g's would still be recorded, while the left side contained only individual 10g accelerometers. This was a preventative measure because test day sea conditions and general vessel response were not well known prior to testing. These accelerometers were mounted by attaching them to small aluminum plates with #4 machine screws then fastening those plates to the skis with double-sided tape.

Figure 5.3. Accelerometers were mounted close to each arch attachment atop the rigid skis. Photo by author, 2011.

Once sensors acting as model inputs were successfully chosen, interesting model outputs had to be carefully selected. For this study the outputs of choice were spring deflections, tri-axial acceleration at the payload tray and relative rotation between the front arch and payload tray. A pair of splash-resistant, 10-inch stroke linear potentiometers was used to measure the deflection of the springs. Such a large stroke was not ideal for this application due to the relatively small rattle space of the suspension, but these were used because of availability. The

potentiometers were installed using custom-milled mounts which allowed for necessary rotation relative to the suspension rocker whilst restricting any translational motion.

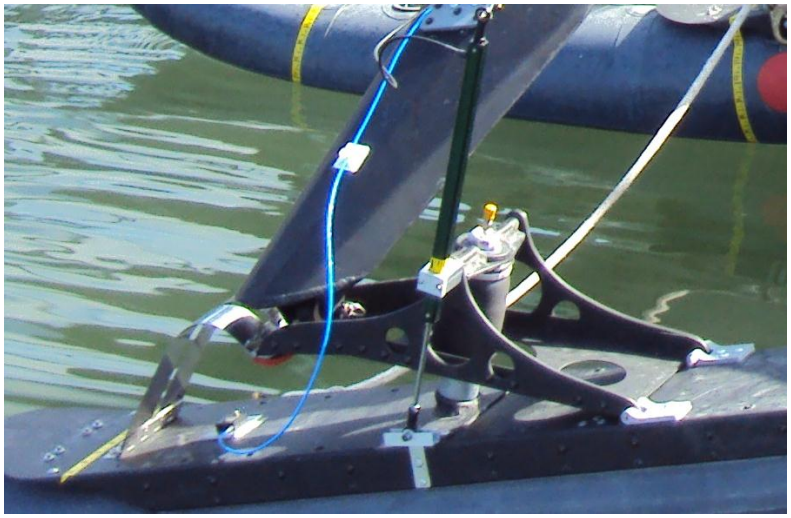

Figure 5.4. Linear potentiometers were used to measure spring deflection while testing. Photo by author, 2011.

Sensor selection for measuring the rotational motion of the front arch with respect to the payload tray proved to be a difficult task. Commonly, rotational displacement is measured using instruments known as rotary potentiometers, which output a proportional voltage with angular deflection. In order to implement a rotary potentiometer, some gearing assembly would have to be designed and manufactured beforehand without ever personally inspecting the vessel, thereby relying solely on images and hand measurements by MAR. This option yielded far too many sources of potential error when being installed on the boat, so a more versatile setup had to be envisioned. The required flexibility came in the form of a string potentiometer; however special attention had to be paid to potential downfalls occurring when applying it in this manner. The first major obstacle is that the string has a restricted stroke depending on the length stored within the potentiometer, thereby limiting the distance away from the pivot that the string could be attached. Then next problem comes in the form of a non-linearity in the relationship between voltage and rotational motion of the arch, which stems from angular deflection of the line of action of the string from its at-rest position. The final solution utilizes a custom mount which optimizes string length and places the string initially tangential to a circle centered at the joint's pivot point. This positioning of the string potentiometer, which can be seen in Figure 5.5,

minimizes any non-linearity present in the signal while still providing over 25 degrees of recordable arch motion in either direction.

Figure 5.5. A string pot was installed using a custom mount to retain linearity of the measurement for both directions of motion. Photo by author, 2011.

The final measurement required for this study was the response acceleration at a point near the front of the payload tray representative of where a passenger might be seated on a larger scaled vessel. Unlike the sensors mounted to the pontoons, however, the accelerometer chosen for this application was tri-axial, allowing for analysis of the chassis reaction in all three directions. Mounting for this sensor was simplified by bolting it directly within the waterproof box as can be seen in Figure 5.6. This placement allowed the sensor to be hard wired directly into the CompactRIO and ensured rigid mounting, which would be difficult to replicate if placed directly onto the payload tray.

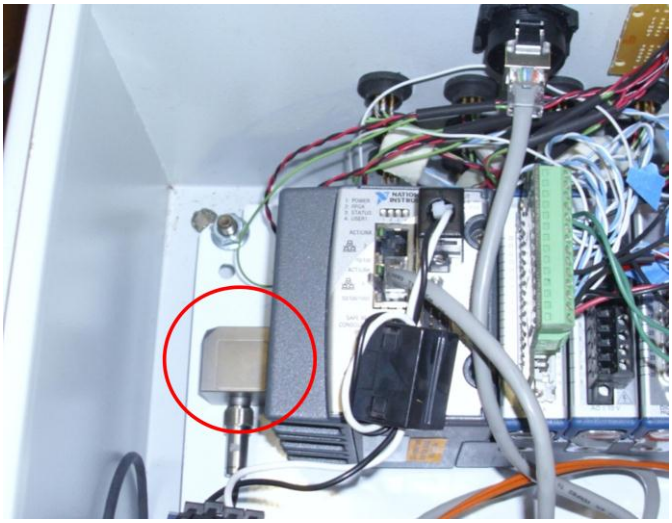

Figure 5.6. The tri-axial cabin accelerometer was mounted directly to the base plate within the water resistant box. Photo by author, 2011.

5.2 Test Setup

Testing was performed on March 11, 2010 on the northeastern reaches of San Francisco Bay proper, departing from the Marina Bay Yacht Harbor in Richmond, CA. Marine Advanced Research aided in this process by providing a chase boat for observation and operating the USV while underway. Per the advisement of employees at the NAVSEA Naval Surface Warfare Combatant Craft Test and Evaluation Division, the testing plan revolved around the iteration of a particular star-like pattern at three different speeds. This pattern helps to ensure that data is recorded with waves striking the boat at a series of important directions. Figure 5.7 and Table 5-1 together summarize the directions of travel for each leg of the star pattern as well as the vessel's magnetic heading for each wave direction during testing. It should be noted that the prevailing wind direction did not change significantly throughout the day of testing.

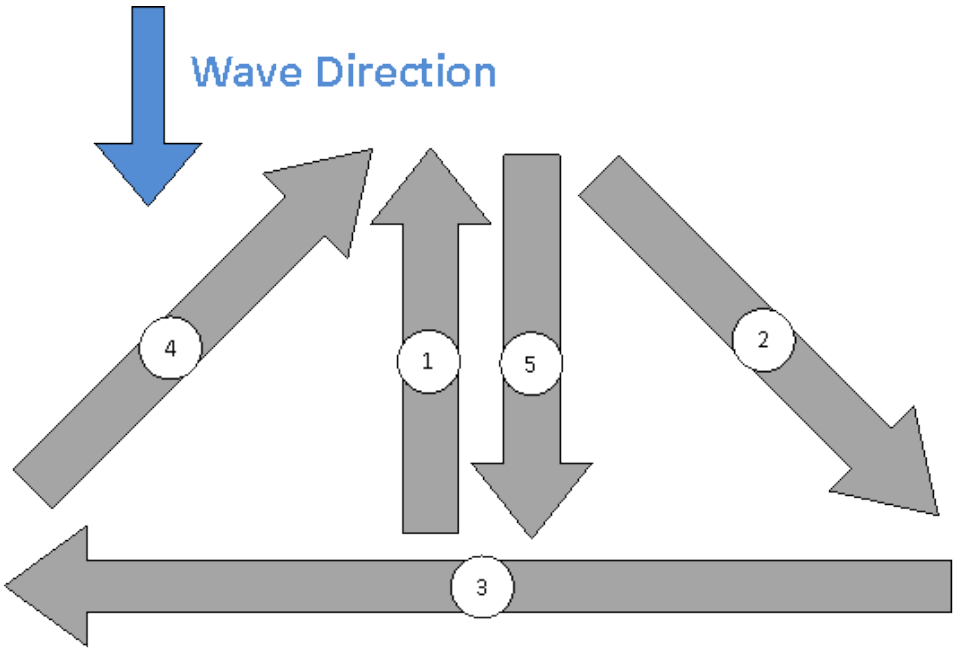

Figure 5.7. A star pattern was utilized to ensure that data was taken with waves striking the vessel at each of five important directions.

Table 5-1

Wave Direction Relative to USV and Vessel Heading per Leg

#	Wave Direction	Heading
1	Head	180°
2	Aft Quartering	315°
3	Beam	90°
4	Bow Quartering	225°
5	Following	0°

Careful documentation is certainly one of the most vital tasks during testing to lead to the successful analysis of data afterwards. To ensure that minimal details were overlooked, redundant systems of note-taking were implemented for this test. Firstly, a MATLAB Graphical User Interface (GUI) was created to automatically record a typed statement along with a timestamp every time a button was pressed. At the completion of a test, this data was written to an Excel file for further analysis. The second method utilized was hand-written documentation including timestamps using a waterproof pen and notebook. Finally, a voice recorder was carried by one member of the team and utilized for supplementary notes and to record any valuable chatter between other members of the crew during testing. These three methods proved

to be very efficient and valuable because three sets of eyes were focused on observing the events as they took place and each recorded separate accounts of them, which could easily be collated to recall those events afterwards.

5.3 On-water Testing

Testing began with packing of the USV at MAR's headquarters. After a short drive north from Berkley to Richmond and assembly of the vessel, the vessel was underway at approximately 10:30 AM. The original testing plan called for three speeds to be analyzed while running through the star patter discussed previously. The first desired speed was 3.5 kts; however it was found that the USV had difficulty holding steady speed with the little throttle required. The first full star pattern was completed at 4 kts, with subsequent full runs at 7 kts and 12 kts before a mechanical engine failure required the team to return to the marina for repairs.

While the vessel was grounded, data from the morning's session was downloaded to a computer and each sensor was checked for nominal operation. During this check it was found that both linear potentiometers fit to the suspension had failed from salt water encroachment into their internals. These sensors were rated to be water resistant to splashes, but it was clear they had succumbed to the incessant spray coming off of the front of each pontoon. Replacement potentiometers were available and were used to replace the broken set with the addition of custom-fit plastic bag splash guards. Although this was not the most ideal protection for the environment these sensors would be in, it was chosen because few other options were available and it was the most time-efficient solution.

After replacement of the linear potentiometers along with a small plastic throttle linkage in one of the engine pods, testing resumed to find slightly rougher sea conditions than were seen in the morning. After making the trek back out into the open bay water and completing one star pattern at approximately 12.5 kts, attempts were made at creating larger false impacts by running the USV back and forth across the chase boat's wake. Several mechanical failures followed while attempting to complete a final star pattern at 12.5 kts further into the bay including water

leaking into an engine pod and a structural pin becoming dislodged from the rear arch. The first three directions of the star pattern were completed in succession followed by a one-hour delay before the final two runs could be performed. A summary of the completed tests can be seen in Table 5-2 below.

Table 5-2

Summary of Events Completed During Testing

Order	Speed (kt)	Event/Notes
1	3.5	• First 2 directions of star pattern completed • Aborted due to unsteady speed
2	4	• Full star pattern completed
3	7	• Full star pattern completed
4	12	• Full star pattern completed
5	12.5	• Full star pattern completed
6	12.5	• First 3 directions completed • 1 hr delay for repairs • Final 2 directions comlpeted

5.4 Model Input Pre-processing

The USV model neglects hydrodynamic effects in the same manner as the Proteus model mentioned in previous sections. This means that the inputs to the simulation would have to be sent as measures of displacement and orientation of the pontoons. As discussed previously, when applying inputs to a SimMechanics dynamic simulation as motions rather than forces, it is required that the motion signal be sent in 3 components: acceleration, velocity and position. This can become a cumbersome task when only one of these is well defined, and it is worst when only acceleration is known. Before sending the pontoon accelerometer data to the model, it was necessary to first remove any mechanical or electronic noise followed by careful integration to determine the proper representative input signals.

5.4.1 Noise Reduction

It was well known from experience and observation of the USV that the pontoon accelerometer signals would contain a large amount of engine vibration noise. In order to properly capture this component of the signal and filter it out, it was necessary to evaluate the signals in the frequency domain. To complete this task, a special strategy was formulated using the well known Fast Fourier Transform (FFT) algorithm within MATLAB. This strategy involves an averaging scheme to help smooth the resultant frequency content and is discussed in the following text.

The FFT algorithm is a method of solving the Fourier Series of any signal and can be computed in as little as one hundredth the time of older Fourier transform solution methods. When a time domain signal is processed by the FFT, a response is produced representing the signal's energy content in the frequency domain between zero and the Nyquist frequency ($^1/_2$ the sampling frequency of the data logger) containing an equal number of data points as the time-domain signal. This can produce a plot with too fine of resolution, resulting in a noisy signal that can be difficult to dissect. One method for reducing the resolution without removing valuable time series data is to average several sets of these frequency responses, each having fewer data points.

Consider for a moment the case of one minute of data from the USV test, which utilized a logging rate of 250 Hz. It follows that the total signal would be of length $n = 15{,}000$. If the frequency content of this signal were to be extracted directly and plotted it would contain 15,000 points between 0 Hz and the Nyquist frequency of 125 Hz, or a frequency resolution of just 0.0083 Hz. The resulting plot at this resolution would appear very noisy, but what would happen if the desired frequency resolution was raised by slightly less than an order of magnitude to 0.08 Hz? In order to find the necessary data set length of each time signal the Nyquist frequency is divided by this desired resolution to get $n \cong 1562$. This means that the original signal can be decimated into nine separate time signals each of length 1562, leaving a remainder of only 942 unused data points from the original signal. The astute reader may notice that if the desired frequency resolution were raised by an exact order of magnitude, then the final signal would be decimated exactly 10 times, thereby leaving zero remaining elements unused. Each of

these signals can then be passed through the FFT algorithm and averaged piecewise at each frequency bin to create the final frequency response. The final frequency spectrum signal is often much easier to analyze, yet contains the entire original time signal. Figure 5.8 depicts a visual representation of the process of frequency domain averaging on a 30,000 point time series.

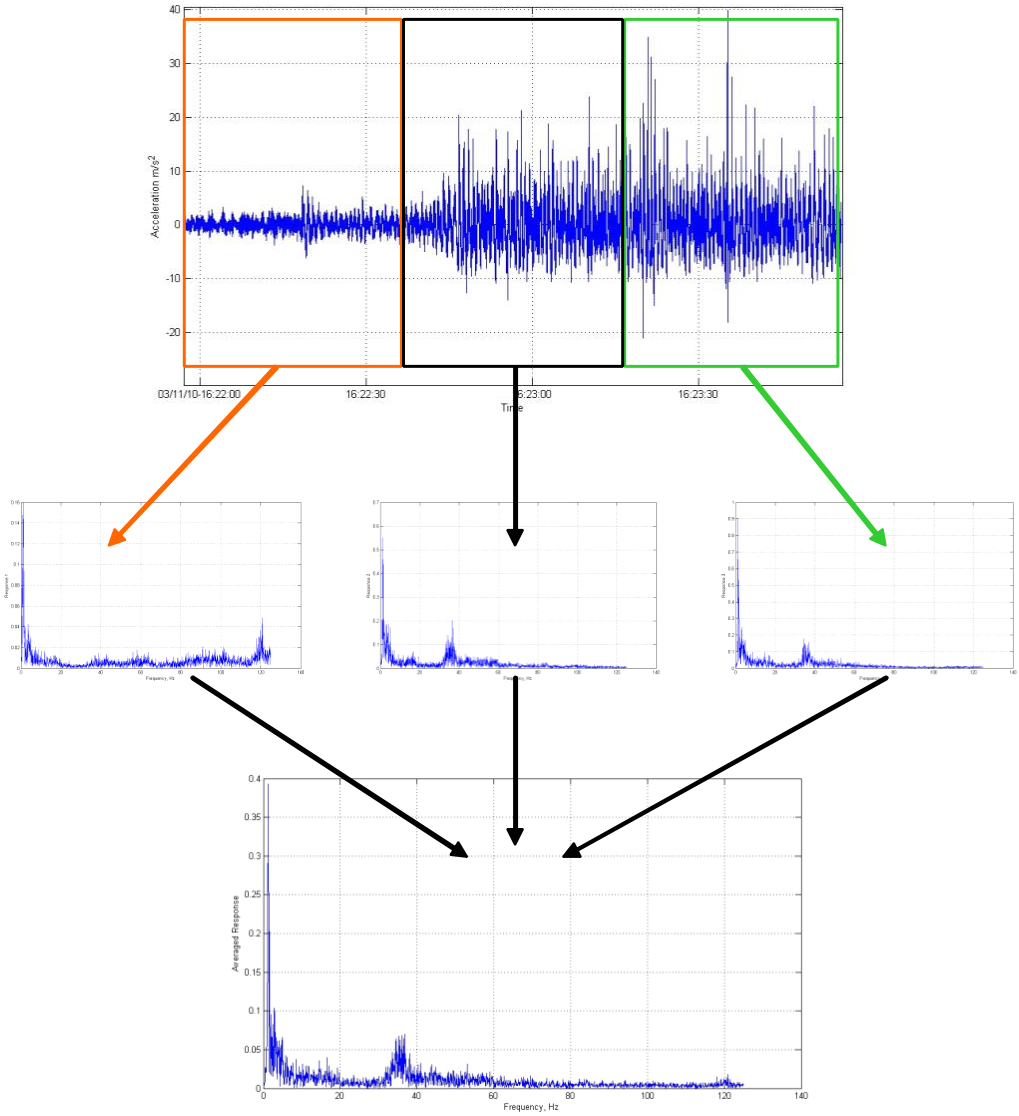

Figure 5.8. This visual example of the FFT averaging scheme utilizes three decimated time series' to collate into the final frequency spectrum.

It was known that engine noise would play a significant role in the signals received from the pontoon accelerometers. By utilizing the extensive documentation gathered while testing, a portion of data was segmented that clearly showcased an engine being started. As can be seen in

Figure 5.9, the firing of the engine is rather obvious even to the naked eye. These signals were then separated and run individually through an FFT to gather frequency content with the engine off and on. Figure 5.10 summarizes this process and shows not only the obvious engine noise, but also where it is dominant across the frequency spectrum.

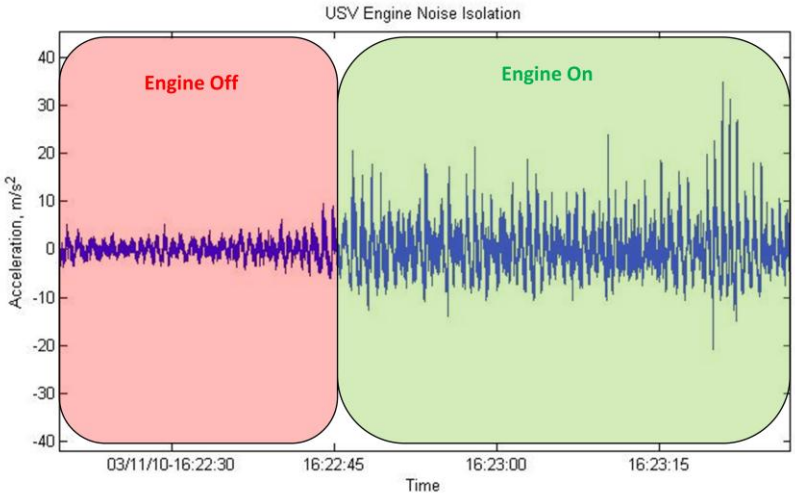

Figure 5.9. A portion of pontoon accelerometer data showing the engine both off and on.

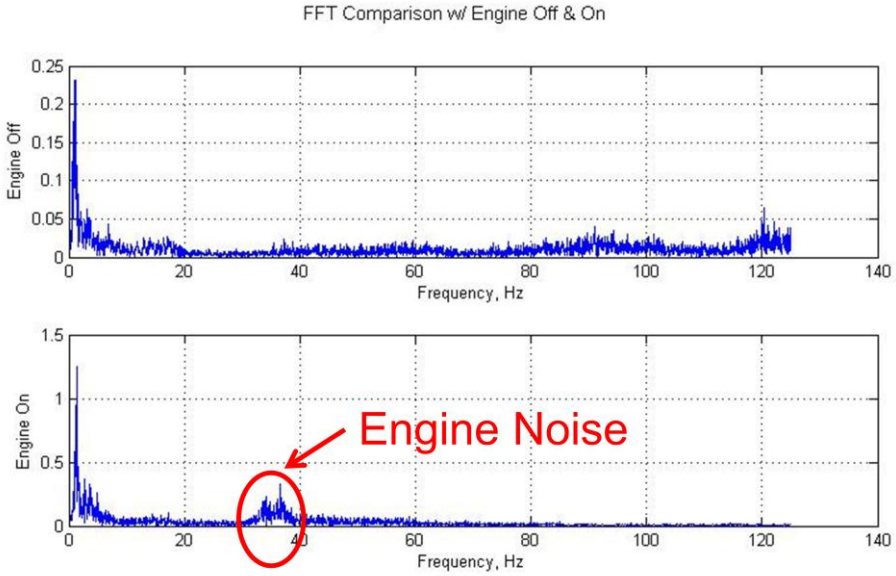

Figure 5.10. The dominant frequencies of the engine noise can clearly be identified.

Once the noise had been clearly identified, it was required that the signals be filtered in an effort to remove the unwanted content. However, it is important when performing a task such as this to ensure that valuable data is not inadvertently filtered out in the process. After

analyzing the frequency content of the signal while the engine was on, it was decided that a lowpass filter with a cutoff frequency at 30 Hz would be suitable for the test. A Butterworth-style filter was chosen because it is maximally flat in the passband of the frequency response. Also, as compared to Chebyshev or elliptical filters, the Butterworth filter does not possess frequency response ripples in either the passband or stopband but has a slightly slower roll-off, requiring the use of a higher order to mimic this characteristic. In this case a 5^{th} order Butterworth filter was chosen to improve the roll-off rate into the stopband.

One issue still remained, however, because any digital filtering of the original time series would result in a phase lag of the resultant signal. Considering that this input data would be used to simulate response characteristics of the USV and then compared to time-series data from testing, it was extremely important to eliminate this potential phase lag. The solution came in the form of a zero-lag filtering scheme in MATLAB called *filtfilt*. This algorithm passes the data through the designed filter twice (once in the intended direction and once in reverse) resulting in zero-phase distortion and a filter order that is double the order of the originally designed filter. This method was utilized for every filter applied to the data throughout analysis.

The ultimate goal of this stage of filtering is to produce clean model inputs, free of any component of engine vibration, while ensuring that the signal's phase content remains unaltered. Figure 5.11 demonstrates this capability by showcasing the left front accelerometer raw and filtered signals in the frequency domain as well as ten-seconds in the time domain. As the first two subplots indicate, the filter does an excellent job of cutting out engine noise. The signal remains visibly unchanged up to approximately 25 Hz before the roll-off becomes evident, leaving the most important part of the signal intact. The final subplot indicates that the zero-phase lag filtering scheme is working as designed. Each wave impact is clearly identifiable and appears to be in phase harmony with the original signal.

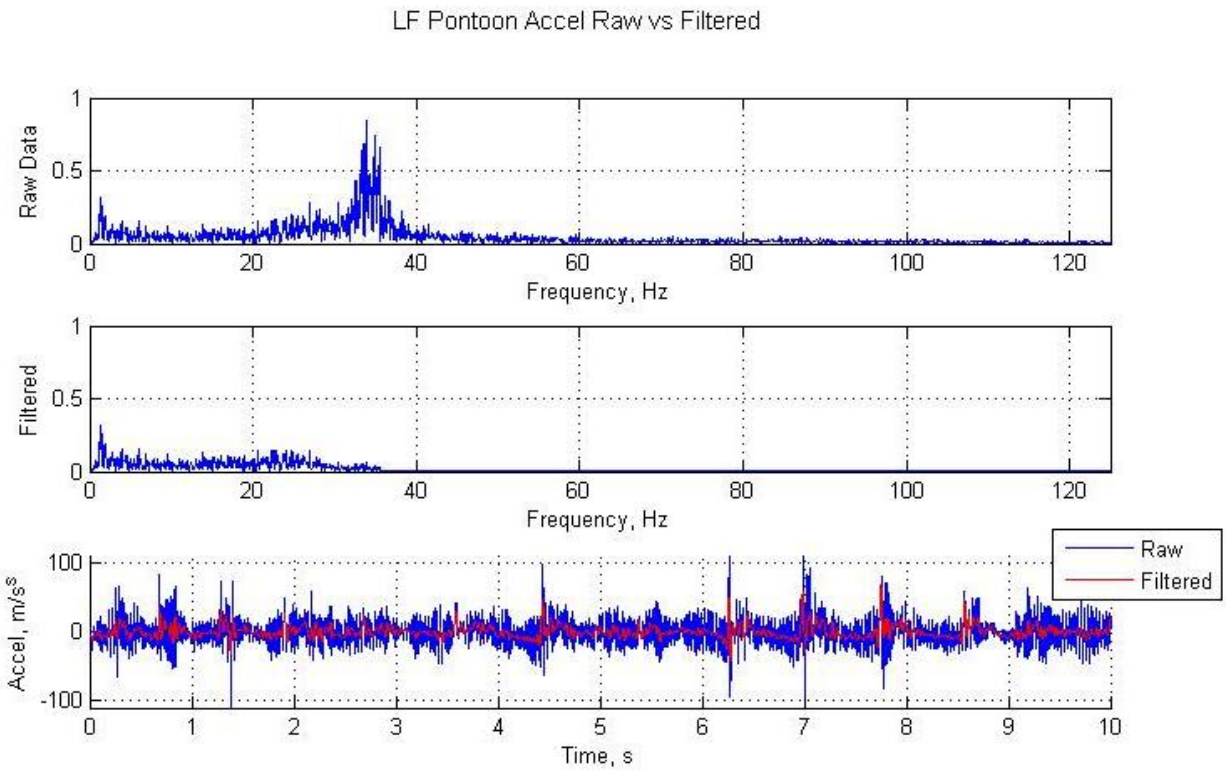

Figure 5.11. The Butterworth lowpass filter clearly eliminates engine noise with little trouble.

5.4.2 Acceleration Integration

As previously mentioned, SimMechanics requires inputs of motion to be three-component signals: acceleration, velocity and displacement. When working with discrete data such as this, it is possible to integrate the acceleration signals with respect to time in either the time domain or frequency domain. When performed in the time domain the integral is solved using a cumulative trapezoidal numerical integration procedure, as taught in any college level calculus course. In the frequency domain, however, the process is simplified into an arithmetic operation.

When a stochastic signal is integrated in the time domain, several forms of error can arise. The most obvious source of integration error comes from the process of discretizing a continuous signal in the first place. Figure 5.12 below displays an example of a continuous signal with a trapezoidal integration overlaid in red. It is obvious from inspection that the results of this integration will contain errors.

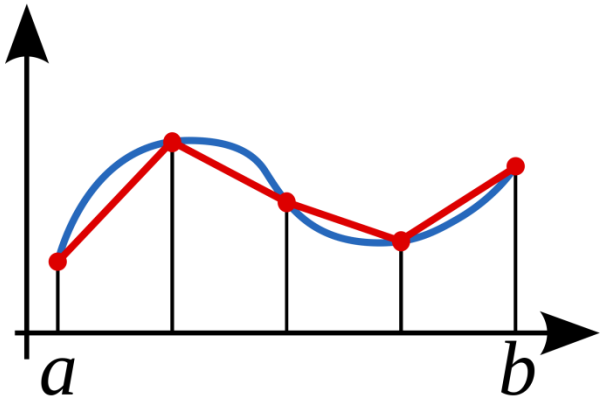

Figure 5.12. Discretization of continuous time-series signals leads to errors when a trapezoidal integration scheme is applied.

Other forms of error, which may not be as obvious, stem from variations in the central tendencies of original signal from zero. When integrated these variations are amplified as can be observed in Figure 5.13. The plots on the left-hand side of this figure represent acceleration signals while those on the right-hand side show their representative velocities after trapezoidal integration. Equations (5-1), (5-2) and (5-3) were used to describe A_1, A_2 and A_3 in the plot:

$$A_1 = \sin(\omega t) \tag{5-1}$$

$$A_2 = \frac{1}{10} + \sin(\omega t) \tag{5-2}$$

$$A_3 = \sin\left(\frac{\omega t}{5}\right) + \sin(\omega t) \tag{5-3}$$

The first signal has a constant mean of zero and is considered the baseline signal. The second and third are variations to this signal with a DC offset and sine-on-sine respectively. It can be observed that the original signal integrates correctly while the second creates a linear drift and the third a sinusoidal drift. The more dangerous of these artifacts to this research is the sine-on-sine phenomenon. The accelerometers utilized for this study operate in the frequency domain down to DC (0 Hz), resulting in a DC-offset due to gravitational acceleration, which is removed before integration. As the pontoons pitch and roll, this gravitational component will change resulting in a similar type of sine-on-sine wave and an amplified error once integrated.

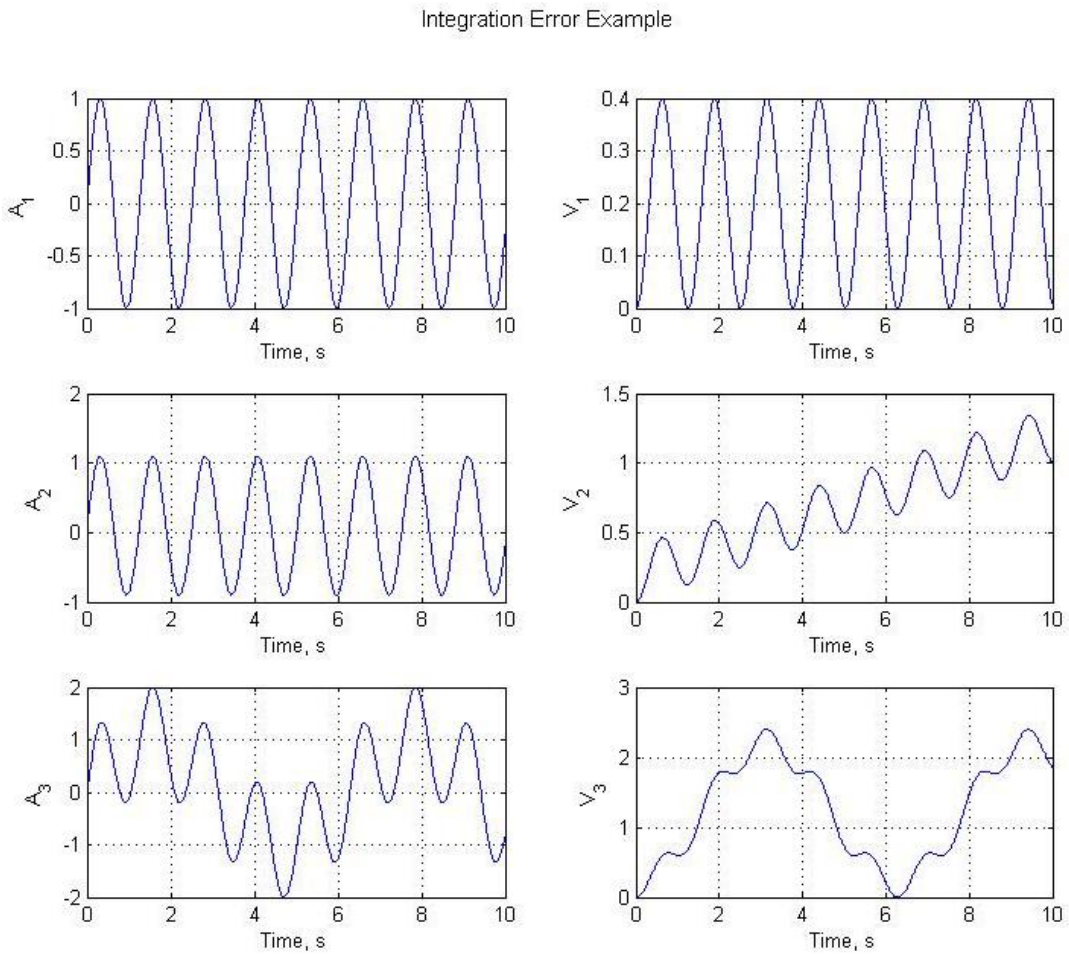

Figure 5.13. Integration error can stem from things such as a DC offset or other dynamic variations in central tendency.

When the same integration process is performed in the frequency domain it solves down to a simple arithmetic equation. Consider a time-series acceleration signal $\ddot{x}(t)$ with frequency content $\ddot{X}(f)$ found by the Fourier transform. This relationship can easily be reversed with the application of an inverse Fourier transform which converts the data from frequency back to time domain. Therefore, the time series of the displacement data could be derived from the frequency content of the displacement data. Conversion of the acceleration signal to displacement in the frequency domain is performed by application of equation (5-4), which is derived in Appendix A.

$$X(f) = \frac{\ddot{X}(f)}{-\omega^2} \tag{5-4}$$

The algorithm behind this equation states that at each individual frequency bin of the Fourier series, the amplitude must be divided by the negative of that bin's frequency squared. This process avoids many of the errors innate to time series integration, but introduces one major downfall at low frequency. The equation displayed above goes to infinity as the frequency approaches zero. This phenomenon is commonly referred to as "$1/f$ noise". In light of the relatively low frequency content of the oceanic inputs and suspension response with respect to the sampling rate, it was concluded that this integration method would not be applicable to the USV testing data.

This decision meant that a reliable technique of compensation for time domain integration error had to be formulated. After several failed attempts, a repeatable method was developed which involved the application of a tuned highpass filter with a very low cutoff frequency pre- and post-integration. Tuning of this cutoff frequency was performed empirically using a very simple test. An accelerometer used during USV testing was mounted to the moving clevis of a Rhoerig damper dynamometer. A string potentiometer was also mounted to the rig to directly measure displacement of the clevis. These two signals were recorded with the same data acquisition system and sampling rate utilized during USV testing to ensure comparable results. A depiction of the testing setup is shown in Figure 5.14 below. In order to fully understand the effects of varying cutoff frequency on this filter, a broad range of testing conditions were planned. The inputs were to be of sinusoidal form, thus varying frequency and amplitude became very important for this test. Table 5-3 outlines the testing procedures planned for calibrating the cutoff frequency of the integration filter. After analyzing the effect cutoff frequency has on integration results, it was decided to utilize a highpass Butterworth filter with a cutoff frequency of 0.35 Hz.

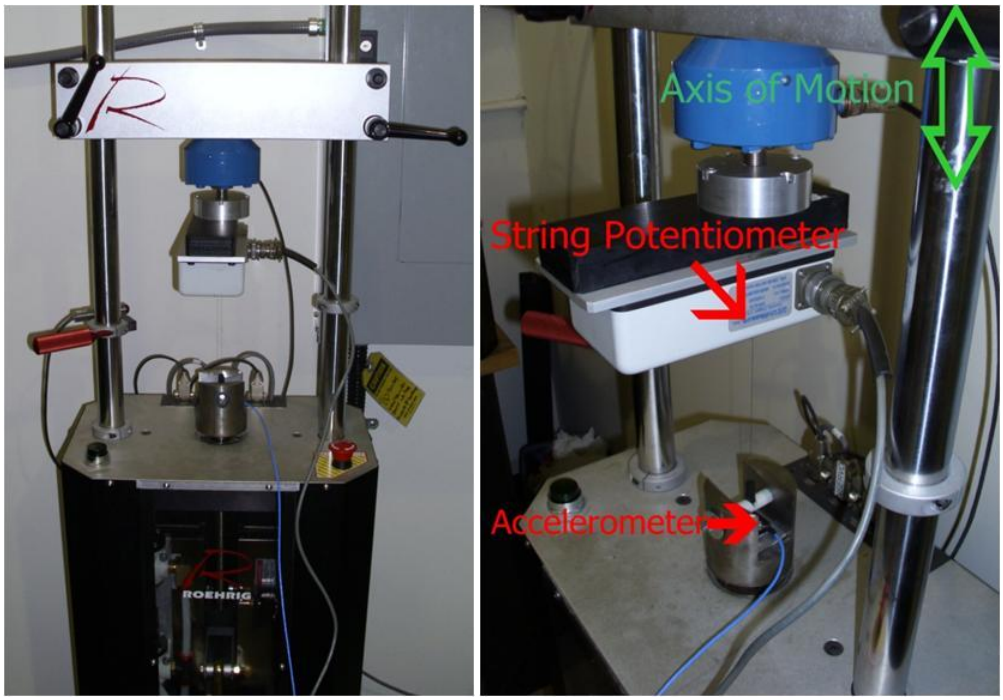

Figure 5.14. A damper dynamometer was outfitted with sensors to gather calibration data for the integration filter. Photo by author, 2011.

Table 5-3

Integration Filter Calibration Test Procedure

		Amplitude (in)			
		7	2	1	0.5
Frequency (Hz)	0.1	3 min	3 min	X	X
	0.2	2 min	2 min	X	X
	0.5	2 min	2 min	X	X
	1	2 min	2 min	X	X
	2	2 min	2 min	X	X
	5	X	1 min	X	X
	10	X	1 min	30 sec	X
	20	X	X	X	30 sec

5.5 Single Degree of Freedom Modeling and Results

When designing a suspension, prediction of the system's natural response frequency is commonly desired or required before anything is built, in order to avoid exciting the system at its resonant frequency. This can become a very difficult task in complex systems, making it valuable to be able to derive this property from simple models. A single degree of freedom (1-DOF) model of the USV was developed by taking the ship in the side view and assuming all chassis motions are purely vertical. Figure 5.15 shows a diagram representing this 1-DOF model where r_1 is the length from rear pivot to front suspension, r_2 is the length from rear pivot to CG, m is suspended mass and k is double the suspension stiffness. Using this model, the natural frequency was derived to be

$$\omega_n = \frac{r_1}{r_2}\sqrt{\frac{k}{m}} = r_r\sqrt{\frac{k}{m}} \tag{5-5}$$

where r_r is defined as the length ratio, which for the case of the USV calculates to 2.14. The full natural frequency derivation for this model can be found in Appendix B.

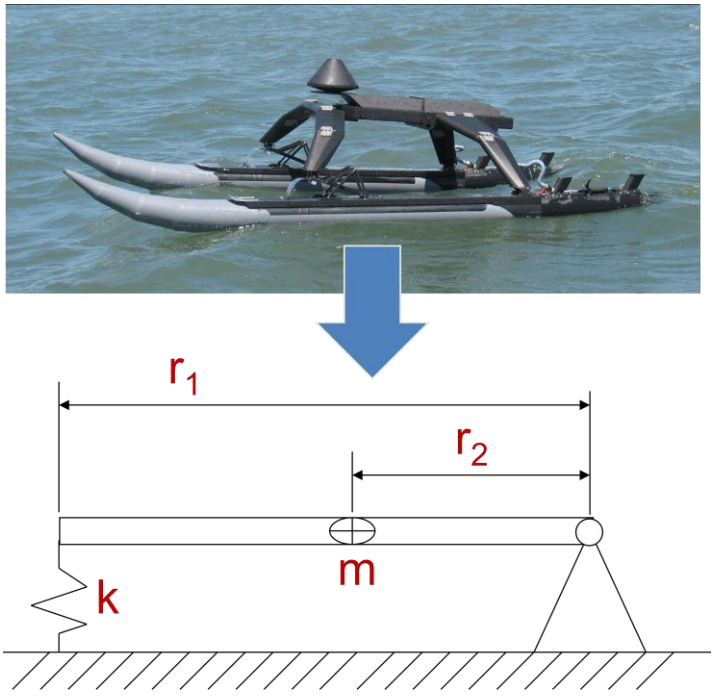

Figure 5.15. A 1-DOF model was developed to predict USV suspension response frequencies. Upper photo by author, 2011.

As discussed in previous sections, the USV spring rate is very nonlinear with displacement. In order to utilize the 1-DOF model, this spring force vs. displacement curve had to be summarized with curve fitting techniques. Several options were considered including 1st, 2nd and 3rd order polynomials and an exponential fit, but the best results came from a combination of 4 - 1st order polynomial (linear) fits as depicted in Figure 5.16. The red and blue numbers within the boxes represent the spring stiffness and relative natural frequency as defined by equation (5-5) above. The numbers located at the bottom of the figure represent statistical displacement percentiles gathered from linear spring potentiometer data during testing. It can be observed that the vast majority of suspension operation is spent at a natural frequency between 2.8 Hz and 3.5 Hz (17th and 95th percentiles).

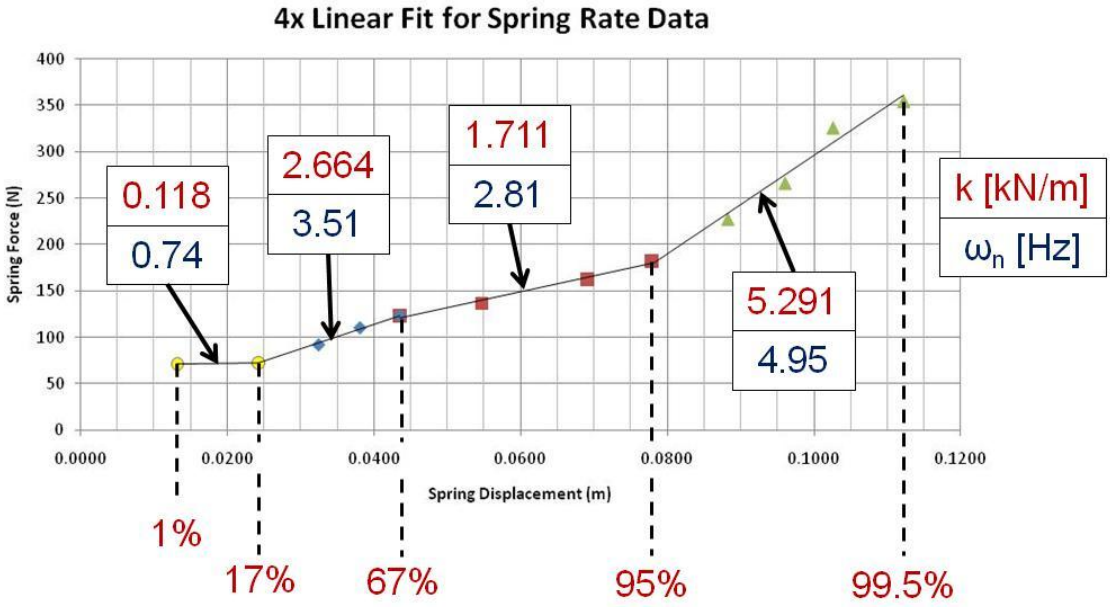

Figure 5.16. The spring force vs. displacement curve was simplified using 4 linear curve fits. The lower numbers in the figure represent statistical displacement percentiles from testing.

Validation of this model required analysis of the frequency content of the spring linear potentiometers. Due to the sensor failures mentioned previously, only a short amount of data was available for this analysis; all of which occurs in head seas at full throttle. Once plotted, the frequency response of the suspension potentiometers reveals interesting results. It is clear in Figure 5.17 that this response contains two major regimes, one at approximately 1.5 Hz and another closer to 3.5 Hz.

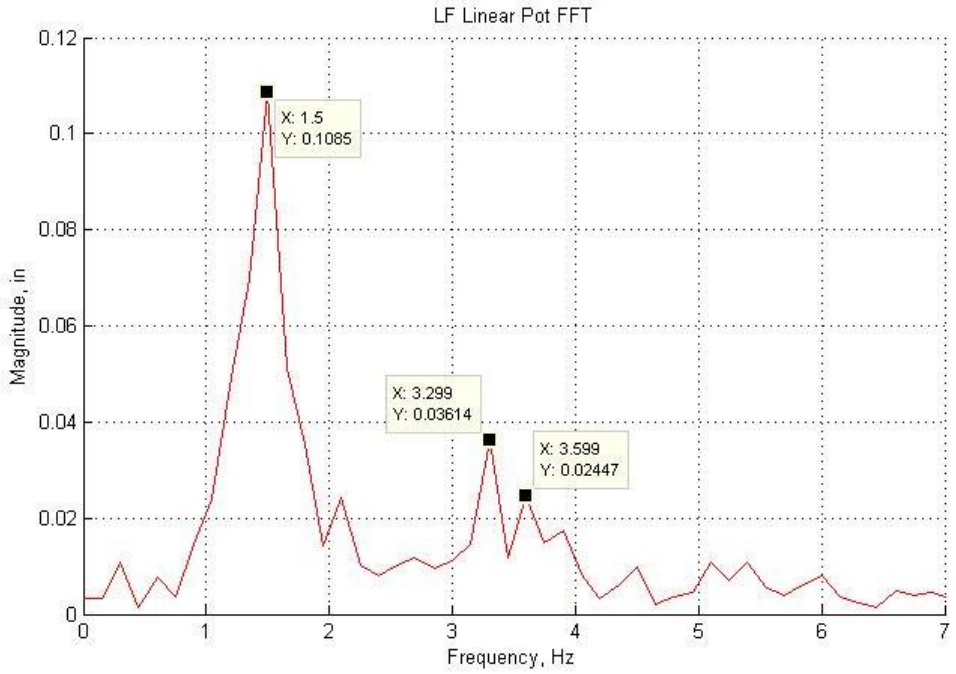

Figure 5.17. The frequency response of the linear spring potentiometer showcases both the input and suspension response frequencies.

It is understood that systems excited at their base, such as the USV, will show oscillatory response with components of both the input and response frequencies. In order to determine which peak belongs to each component, the data was further analyzed in the time domain. Figure 5.18 depicts two seconds of displacement data from the left front linear spring potentiometer, where negative displacement indicates compression of the spring. In this figure very large repetitive peaks at a fairly slow frequency are observed, each being followed by smaller amplitude oscillations. These large peaks should represent individual wave impacts with the ancillary suspension response resulting just afterward. With this assumption in mind, Figure 5.19 reveals that the wave impact frequency range revolves around approximately 1.5 Hz while the response frequency ranges from 2.9 Hz to 3.6 Hz. This outcome confirms the notion aroused by the 1-DOF model results claiming a natural frequency range between 2.8 and 3.5 Hz.

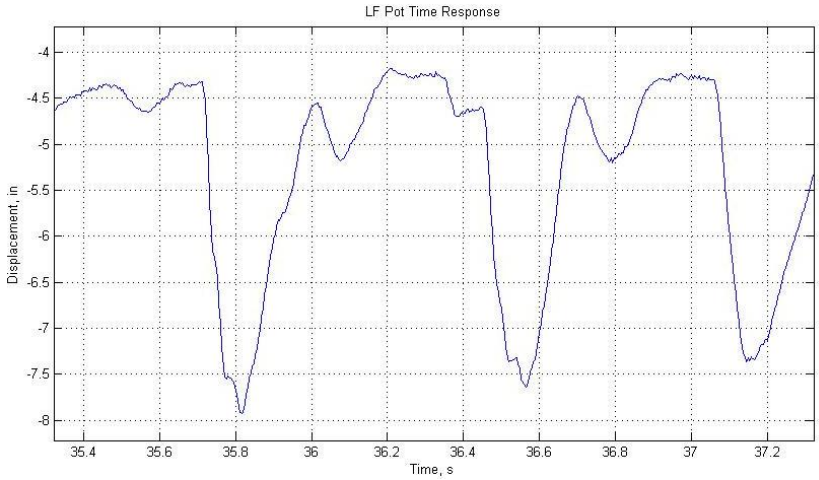

Figure 5.18. Two seconds of linear spring potentiometer displacement data displaying both the impact and suspension response frequencies.

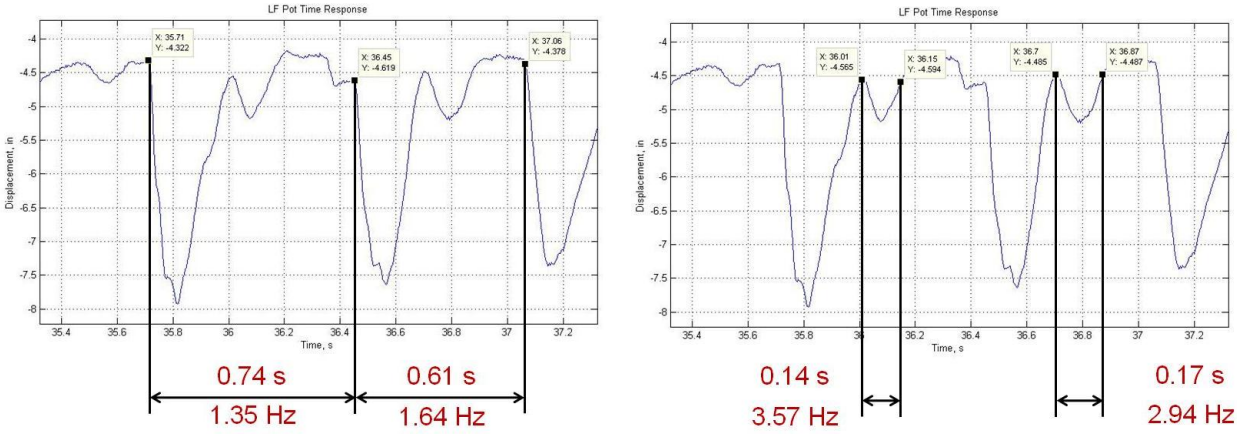

Figure 5.19. As the data from Figure 5.18 is manually analyzed, it reveals the same frequencies found from the Fourier analysis.

5.6 Multi-Body Dynamic Simulation Results and Validation

As discussed previously, the validation of simulation models is a critical step in the application of those models into dynamic prediction algorithms. Validation of the USV multi-body dynamic model was performed primarily in the time domain. Great emphasis was placed on ensuring phase correlation between measurement and simulation, thus it was felt that analysis in the time domain would best test the robustness of the model.

The first step in assessing the validity of the dynamic simulation was to investigate the estimated linear damping rate as discussed previously in section 4.4. The USV model was simulated at six different damping coefficients and responses were recorded for several interesting parameters. Table 5-4 summarizes the damping coefficients and the corresponding percentages from baseline used. For this analysis, the right front suspension displacement, right front suspension velocity, and center of gravity vertical acceleration are displayed in the time domain for each of the damping coefficients summarized below. Figures Figure 5.20, Figure 5.21, and Figure 5.22 show the responses, respectively. Each figure is organized in the same order as shown in Table 5-4.

Table 5-4

Linear Damping Coefficients Tested for Assumption Validation

Damping Scenario (% of Baseline)	**Damping Coefficient** $\left(\frac{\boldsymbol{N-s}}{\boldsymbol{m}}\right)$
33 %	10
66 %	20
Baseline	30
200 %	60
300 %	90
400 %	120

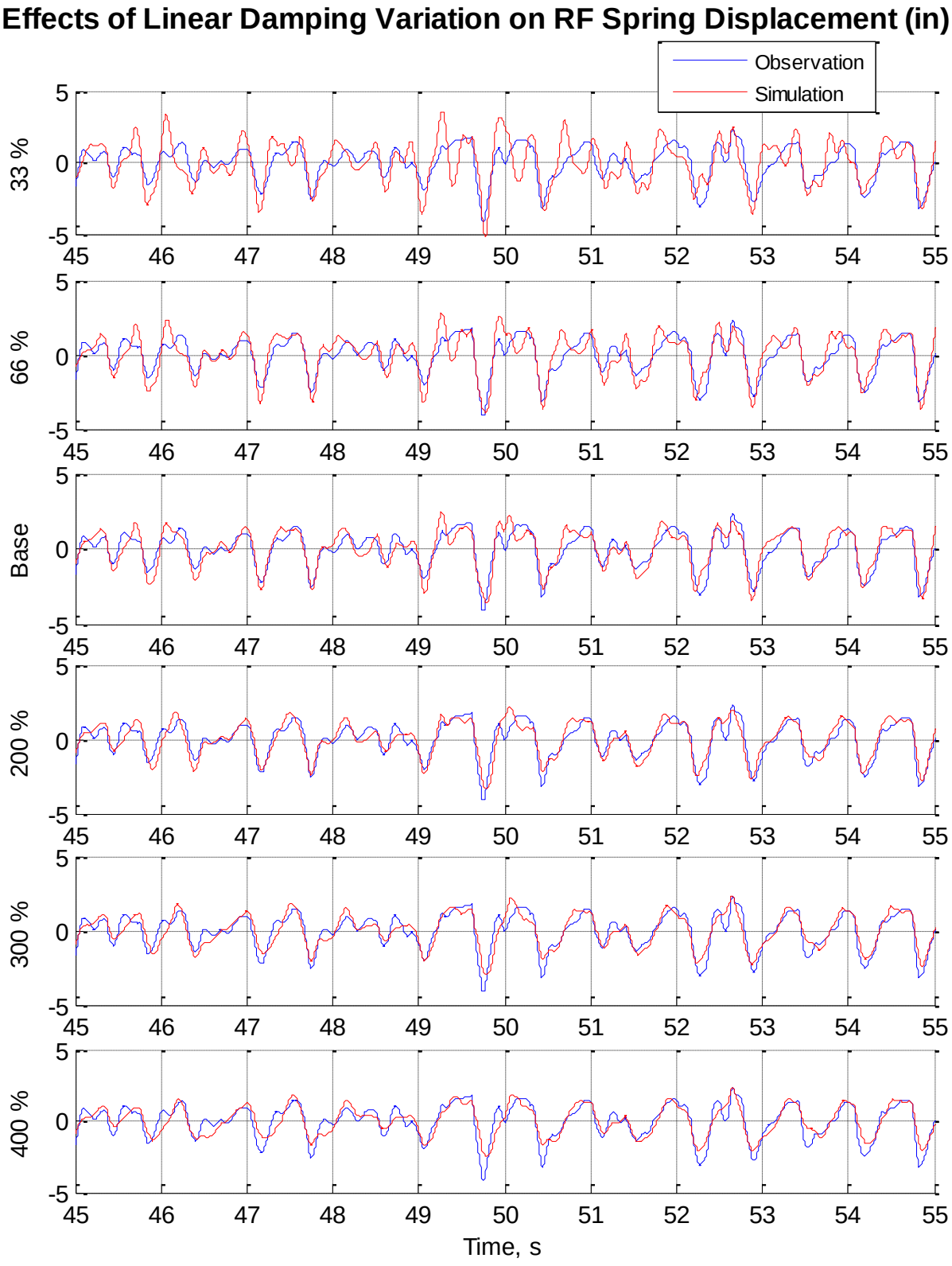

Figure 5.20. Variation of right front spring displacement response due to damping coefficient.

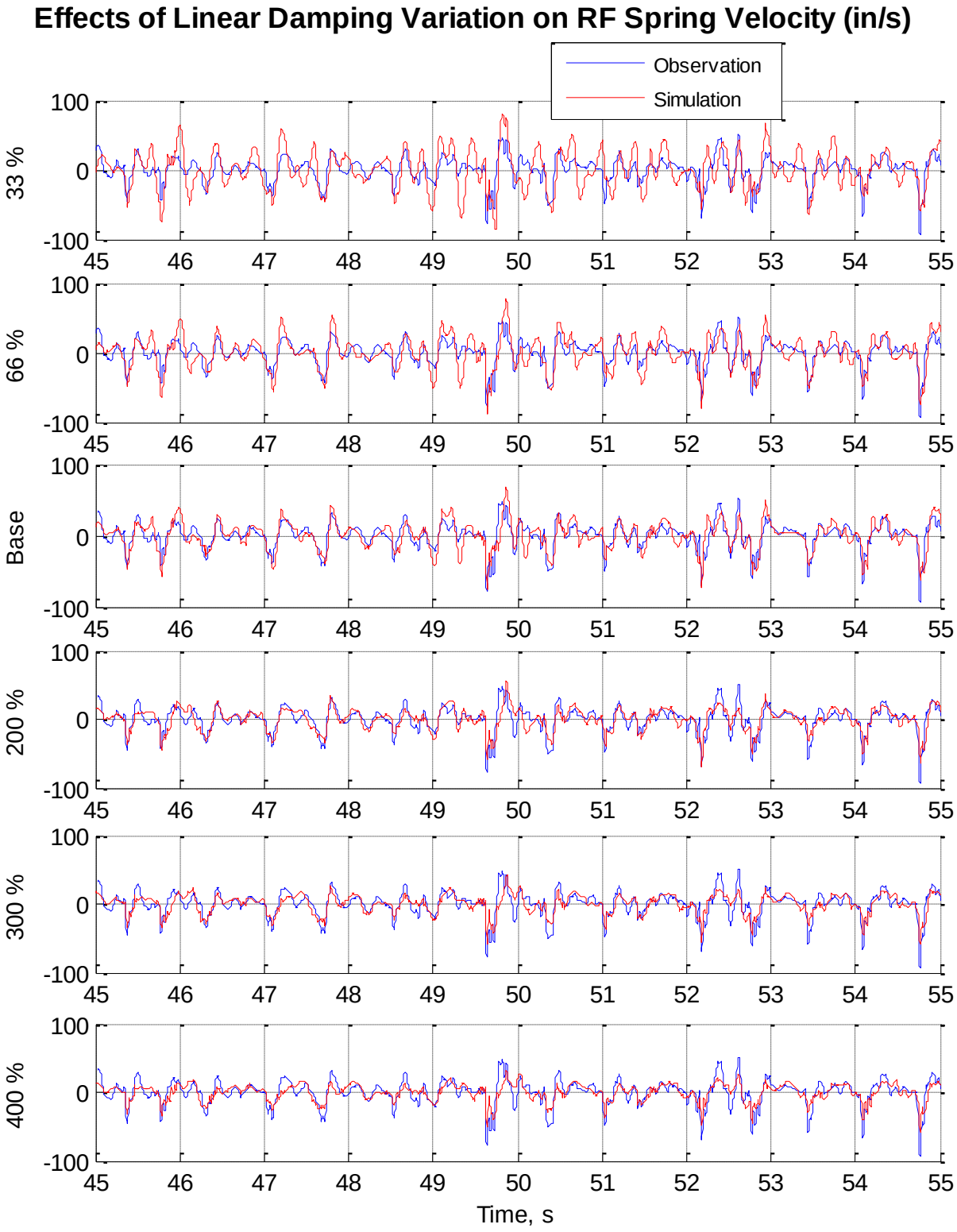

Figure 5.21. Variation of right front spring velocity response due to damping coefficient.

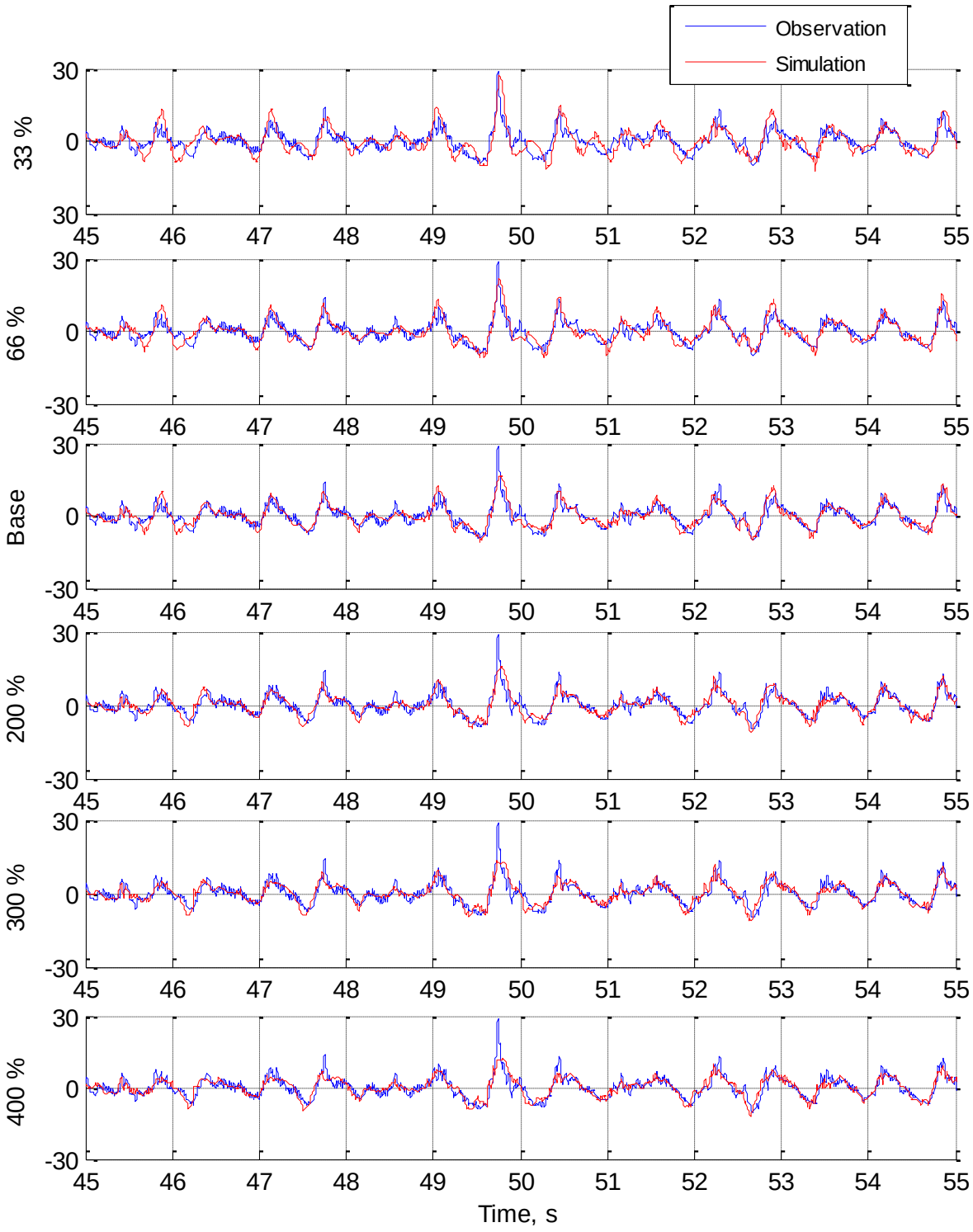

Figure 5.22. Variation in center of gravity vertical acceleration response due to damping coefficient.

As would be expected, the lightly damped simulations exhibit increased overshoot and oscillatory motions not present in the measured data while the heavily damped responses are slow to respond and show some undercutting of observed peaks. This is more prevalent in the right front suspension displacement and velocity responses of Figures Figure 5.20 and Figure 5.21 than the vertical acceleration response of Figure 5.22. The most obvious changes can be seen in the velocity response, which makes sense because this motion directly drives the damping forces of the vessel. The displacement response shows a much greater effect when the damping is reduced from baseline rather than increased. When browsing the response traces from vertical acceleration, however, these same trends become much more difficult to find. At extrema, such as the 3g peak just before 50 seconds, the effects can be identified, but most other areas in the time series are very insensitive to changes in damping. Cabin vertical acceleration response is probably the most important value to be able to predict for this study and this model seems to be very robust in that manner. It should be noted that despite any sensitivities of the model to damping variation, the estimated baseline damping coefficient developed in section 4.4 produces extremely accurate results for all three motions.

The next step of the validation process was to directly compare the simulated and actual response of several output sensors. Figure 5.23 represents the cabin acceleration, central joint rotational displacement and both suspension displacements for 10 seconds. Measured data is represented in blue with simulated data in red. From a general perspective, all of the simulated responses appear to readily emulate the measured responses from the test vessel.

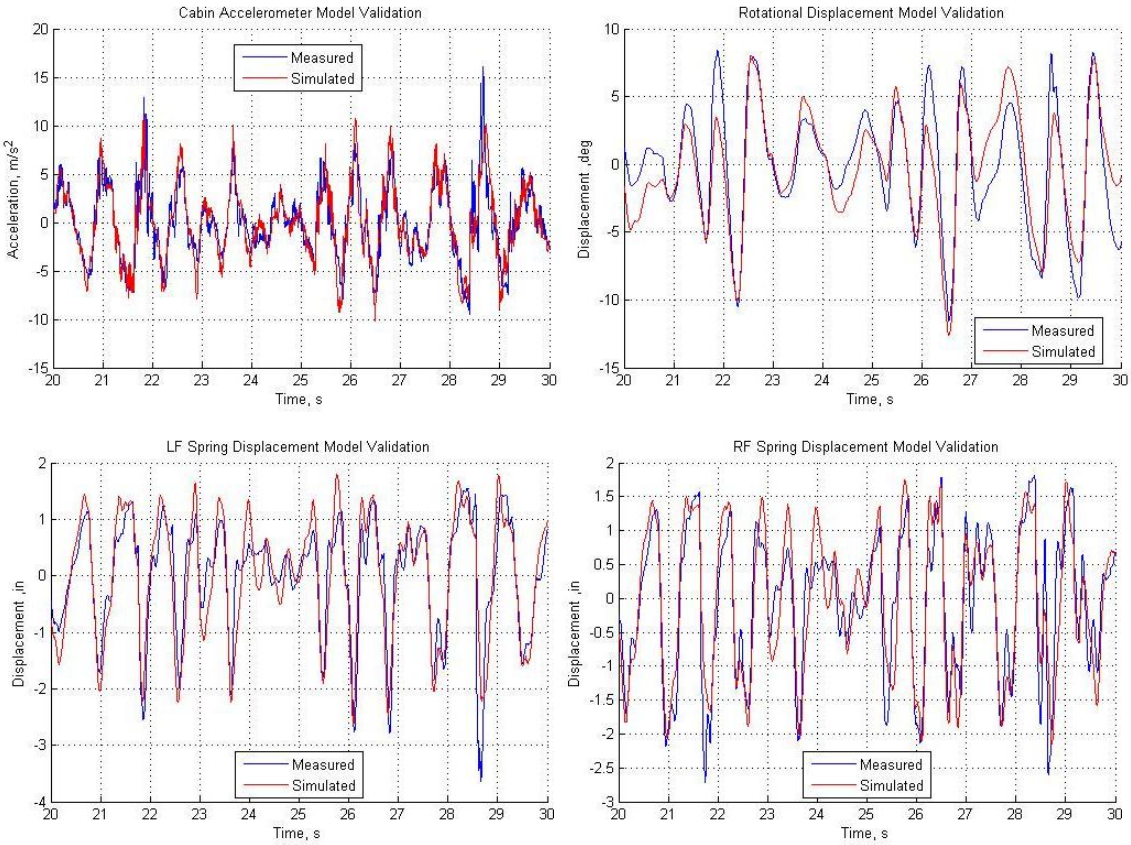

Figure 5.23. In the time domain the USV simulation appears to very accurately represent the realistic testing measurements.

The most accurate fitment of reality to simulation comes from the cabin accelerometer. This is very promising because this reading is one of the most important to be able to properly simulate. Both the left and right suspension potentiometer figures at the bottom show extremely well matched results while the rotational measurement of the top right shows slightly greater error, but very promising response trends.

Chapter 6

Concluding Remarks

During the course of this research, two dynamic simulation models were created in SimMechanics. The kinematically constrained Proteus model successfully produced common trends associated with particular parameter variations. The simpler USV dynamic model was validated in the time domain with test data. This data was used to create representative inputs to the model and as a comparison to simulated outputs. The following chapter will highlight the successes and shortcomings of these models, simulations, and studies and provide recommendations for future research in this field.

6.1 Summary and Discussion

6.1.1 Parametric Analysis of Proteus

The Proteus dynamic simulation model worked well as a tool to predict trends resulting from variations in important dynamic parameters, but also had several drawbacks. Due to the method in which the Proteus dynamic model was imported from CAD, the kinematics could not be varied. This limited the parametric analysis from delving into the effects of variations on basic ship architecture and only allowed for the study of spring rates, damping coefficients and mass properties. This restriction, however, comes with the benefits that the kinematic constraints and baseline mass and mass location are very accurate. It should also be noted that these results did not come from stochastic ocean inputs, but rather from simple periodic waves. Pure heave and pitch modes are idealized cases where the vessel speed, wave speed and wavelength are matched perfectly under head sea conditions. Any real oceanic input, even in the head sea direction, will most likely result in some combination of all four excitation modes.

The heave excitation will produce the best results for analyzing the effect that the suspension has directly upon the cabin motion. When the vessel is driven in other modes, more kinematic relationships come into play with the cabin response. This is obvious due to the fact that the vertical CG position plays a drastically more significant role on the vertical acceleration from pitch than heave. Also, the increased absolute sensitivity of the rear spring rate from pitch excitation as sensed by the rear accelerometer indicates that this effect may be taking place. In general, the sensitivity results match up to common sense results very well. As can be seen in the summary of parametric analysis findings presented in Table 6-1, the springs play the greatest role on accelerations felt closest to that suspension, while the mass properties affect the areas closest to the sprung mass CG. It should be noted that the variation of damping provided negligible effects on response, which could be a result of the minute baseline damping coefficient.

Table 6-1

Summary of Parametric Analysis Results

Parameter	**Primary Relation**	**Most Sensitive Position**
Spring Rate	Inverse	At end closest to the relative suspension
Mass	Direct	Closest to sprung mass CG
CG Long	Inverse	Closest to sprung mass CG
CG Vert *	Direct	Closest to sprung mass CG

* Indicates that this parameter is only sensitive under pitching excitation

These trends should be indicative of parametric variations of any vessel very similar to Proteus, but the results also must be taken with a grain of salt. The springs on Proteus are

extremely non-linear and all damping is a result of friction in the joints and sliding members. In the parametric model, these effects are assumed to be completely linear. Because of this, the simulated percentage sensitivities are probably not indicative of the results as they would be seen on Proteus because of the effects of non-linearity, however the trends and primary relationships should hold true.

6.1.2 USV Modeling & Validation

The validation results from the stochastically excited USV dynamic model show excellent agreement to testing data. Although this model appears to be very simple in comparison to the detailed Proteus model it retains a high level of accuracy for the most important properties including mass, CG location, spring rates, and polar inertia in primary directions of rotation. The USV dynamic simulations run very quickly and are an excellent substitute for costly and time-consuming testing. The single-DOF model also showed a great deal of agreement with testing data in the frequency domain. This proved the validity of the spring rates being applied to the dynamic model and gave insight into the primary range of motion and natural response frequencies of the vessel.

The major limitation of the dynamic USV model, however, comes from the method in which the inputs were applied. By choosing to neglect hydrodynamic effects the inputs to the model were required to come from data collected directly on the pontoons of a test vessel. This condition is a result of the codependent relationship between any hull and the water it is passing through. As the hull is being affected and moved by a passing wave, it is also physically degrading the local wave structure. This essentially means that the model inputs are limited in scope to only properly excite the specific USV arrangement. Any change in basic configuration or major parameter alteration would lead to a different water/hull response dynamic and would produce different inputs at the pontoons.

The time-series results of the USV model validation are extremely promising. Although the input data is being filtered and integrated several times, the outputs match the test data remarkably well in amplitude, shape, and phase. The most promising results come from the vertical acceleration at the cabin. This is the most important signal to match for analyzing

passenger comfort and shows the tremendous prediction power of the USV SimMechanics model. Both suspension potentiometers also reveal excellent response matching. The slight error between the measured and simulated linear potentiometer signals could be the result of the assumptions made when deriving the spring force characteristics from the raw data or minor errors coming to the surface from the integration and filtering of the inputs. The worst matched dataset is the relative rotational displacement of the front arch with respect to the payload tray. Even this signal, however, produces very well matched results with the increase in error potentially coming from several factors including those mentioned above for the linear potentiometer error as well as the probable fact that some components' polar inertias in the simulation did not match their respective parts on the real vessel as well as was initially hoped.

6.2 Recommendations

Further simulation development of WAM-Vs™ will be required before its full benefit can be realized. As stated previously, the primary limiting factor of the dynamic model in its current state is the lack of a hydrodynamics solver. The model showed excellent capabilities to predict chassis motions so long as reliable inputs could be applied. Without the ability to solve for the water/hull interaction the scope of these simulations will limit them from their true potential of replacing expensive on-water testing.

Although the USV model provided acceptable enough results to prove its potential validity, the breadth of comparable testing data was extremely limited. Future testing should include variations in suspension stiffness and damping, payload mass and location, and even basic ship configuration. This enlarged scope should provide the necessary data to ensure the validity of dynamic simulations to predict WAM-V™ motions. In addition, the multitude of parameter variations would provide an excellent basis for tuning model parameters, thereby increasing prediction accuracy.

Future WAM-V™ testing platforms should be made adaptable for "locking out" particular components such as the suspensions or main ball joint. The relationship between

simple catamarans and WAM-Vs™ is not well known at this time; therefore the impact of each architectural variant on the change in vessel response needs research. Having the ability to essentially eliminate particular systems and to even force the configuration to be a simple catamaran supplies the user with insight into the effect of each component onto the total vessel response. This information could be used as a guide for resource allotment in the design of future WAM-Vs™.

The final recommendation for future testing of WAM-Vs™ is to make an effort to study the difference in response of the vessel to ocean swell (ground swell) and wind swell. Ocean swell originates from far-off storms or wind-systems and results in waves that are very stable in their direction and frequency whereas wind swell comes from local winds and produces more chaotic waves with faster and more variant frequency. These two excitation sources could produce very different results, but both need to be understood. This could easily be achieved with testing in open-ocean followed by a bay or other body which is protected from ocean swell, but large enough to show significant wind swell.

Appendices

Appendix A

Acceleration Integration – Omega Arithmetic

Let us define $\ddot{x}(t)$ and $\ddot{X}(f)$as the time- and frequency-domain acceleration signals, respectively. The frequency spectra of any time-based signal can be found with the Fourier transform, which can also be inverted to revert back from the frequency to time domain. Using the inverse Fourier transform, the following relations can be made for acceleration, velocity and displacement.

$$\ddot{x}(t) = \int_{-\infty}^{\infty} \ddot{X}(f) e^{2\pi i f t}\, df$$

$$\dot{x}(t) = \int_{-\infty}^{\infty} \dot{X}(f) e^{2\pi i f t}\, df$$

$$x(t) = \int_{-\infty}^{\infty} X(f) e^{2\pi i f t}\, df$$

Using these relationships, the association made between velocity and acceleration in the time domain can be extended into the frequency domain.

$$\ddot{x}(t) = \frac{d}{dt}[\dot{x}(t)]$$

$$\begin{aligned}\ddot{x}(t) &= \frac{d}{dt}\left[\int_{-\infty}^{\infty} \dot{X}(f) e^{2\pi i f t}\, dt\right] \\ &= \int_{-\infty}^{\infty} \dot{X}(f) \frac{d}{dt}\left[e^{2\pi i f t}\right] df \\ &= \int_{-\infty}^{\infty} 2\pi i f \dot{X}(f) e^{2\pi i f t}\, df\end{aligned}$$

When this results is compared back to the Fourier transform representation of $\ddot{x}(t)$ it can be seen that

$$\ddot{X}(f) = 2\pi i f \, \dot{X}(f)$$

$$\dot{X}(f) = \frac{\ddot{X}(f)}{2\pi i f} = \frac{\ddot{X}(f)}{i\omega}$$

When this concept it applied to the conversion from displacement to acceleration, the following results is found.

$$\ddot{X}(f) = -(2\pi f)^2 X(f) = -\omega^2 X(f)$$

Appendix B

USV Single-DOF Model

To analyze the natural response frequency of the USV chassis a basic single-DOF model was created. The USV was modeled as a beam pinned at one end and sprung at the other. The diagram of Figure B-1 displays this simplified representation for the USV chassis dynamics. By creating a balance of moments about the pivot point an equation of motion can be created to find the natural response frequency.

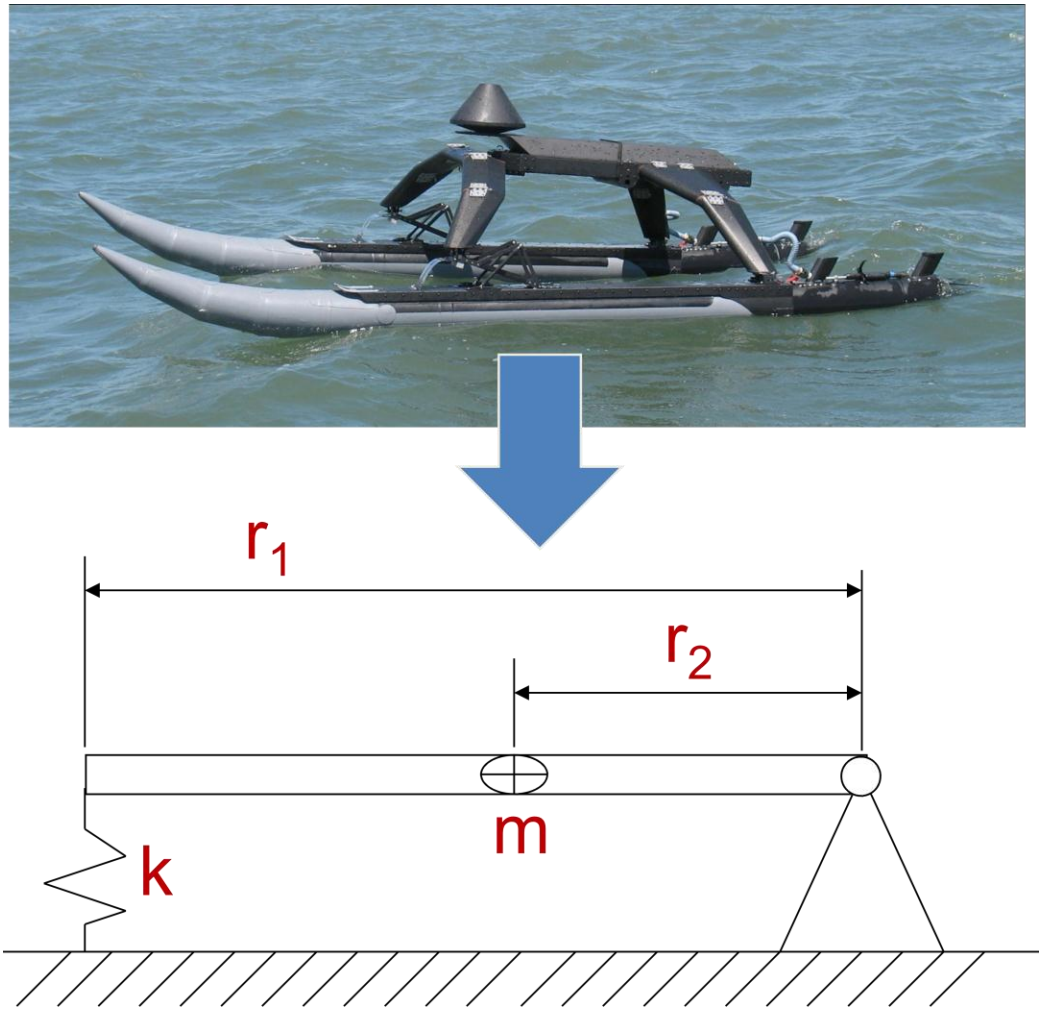

Figure B-1. The USV was modeled as a pinned-and-cantilevered beam with a spring opposite the pin. Upper photo by author, 2011.

By utilizing the small-angle assumption the following equations spell out the derivation for solving the USV natural frequency.

$$\sum M_O = I\alpha$$

$$I = m(r_2)^2$$

$$\sum M_O = -F_k r_1$$

$$F_k = kr_1\theta$$

$$\sum M_O = -k(r_1)^2\theta = m(r_2)^2\ddot{\theta}$$

$$m(r_2)^2\ddot{\theta} + k(r_1)^2\theta = 0$$

$$\omega_n = \sqrt{\frac{k(r_1)^2}{m(r_2)^2}} = \frac{r_1}{r_2}\sqrt{\frac{k}{m}}$$

For the USV case, $r_1 = 1.397\ m$ and $r_2 = 0.653\ m$, therefore

$$\omega_n = 2.14\sqrt{\frac{k}{m}}$$

References

[1] Baitis, A. E. et al. 1975. "A Seakeeping Comparison Between Three Monohulls, Two Swaths, and a Column-Stabilized Catamaran Designed for the Same Mission." *NTIS* (July).

[2] Bautista, J., Kuehne, H., Irvine Jr., M., & Riley, M. 2009. "Marine Advanced Research WAM-V PROTEUS Propulsion, Seakeeping, and Miscellaneous Trials." Naval Surface Warfare Center Carderock Technical Memorandum. NSWCCD-23-TM-2009/43.

[3] Bonafoux, J., Edward Dudson, and D. Sherwood. 2001. "An Evaluation of the Effect of Hull Form Choice on the Operability of Fast Ferries." *Fast 2001 Conference*. Southampton, England, September.

[4] Bulian, Gabriele, and Alberto Francescutto. 2008. "Large amplitude rolling and strongly nonlinear behaviour of multihull ships in moderate beam waves." *IUTAM Symposium on Fluid-Structure Interaction in Ocean Engineering*.

[5] Clark, Dennis J, William M Ellsworth, and John R Meyer. 2004. "The Quest for Speed at Sea." *NSWC Carderock Division - Technical Digest*: 3-27.

[6] Davis, M R, and D S Holloway. 2003. "The influence of hull form on the motions of high speed vessels in head seas." *Ocean Engineering* 30: 2091-2115.

[7] Dubrovsky, Victor, and Konstantin Matveev. 2005. "New Types of Sea-Going Multi-Hull Ships with Superior Comfort Level and Safety." *Passenger Vessels for the New Millenium: Joint Meeting of the Pacific Region Sections*: 1-12.

[8] Dyachkov, Vasilij, and Jurij Makov. 2005. "Seakeeping of a fast displacement catamaran." *Transport* XX(1): 14-22.

[9] Fang, C.C., and H.S. Chan. 2004. "Investigation of Seakeeping Characteristics of High-Speed Catamarans in Waves." *Journal of Marine Science and Technology* 12(1): 7–15.

[10] Kos, Serđo, D. Brčić, and Vlado Frančić. 2009. "Comparative Analysis of Conventional and SWATH Passenger Catamaran." *Proceedings of International Conference on Transport Science*. Portorož, Slovenia. p. 4–5.

[11] Nagai, Tamotsu. 1987. "Critical Review of SWATHs." *Research Reports of Ikutoku Tech. Univ* B-11: 1-21.

[12] Thomas, G., P. Tomic, and a. Tuite. 2007. "High-speed catamaran or monohull? How do you choose?" *Ships and Offshore Structures* 2(2): 137-147.

[13] Turan, Osman, Chirstos Verveniotis, and Hassan Khalid. 2009. "Motion sickness onboard ships: subjective vertical theory and its application to full-scale trials." *Journal of Marine Science and Technology* 14(4): 409-416.

[14] Varyani, K. 2000. "Motions and slamming impact on catamaran." *Ocean Engineering* 27(7): 729-747.